Visualizing turnover of synaptic vesicle protein Synaptogyrin/SNG-1 in vivo using a new method, ARGO (Analysis of Red Green Offset)

Nikita Shiliaev[1], Sophie Baumberger[1], and Claire E. Richardson[1,2]*

[1]Department of Genetics, University of Wisconsin-Madison
425-g Henry Mall, Madison, WI, 53706-1580 USA

*Corresponding author: claire.richardson@wisc.edu

Running head: Visualizing synaptic vesicle protein turnover in vivo

Keywords: Presynapse maintenance, protein turnover, protein half-life, fluorescence microscopy, synaptic vesicle

Abstract

Proteostasis is critical for cellular function and longevity, especially in long-lived cells including neurons. A major component of proteostasis is the regulated degradation and replacement of proteins to ensure their quality and appropriate abundance. The regulation of synaptic vesicle protein turnover in neurons is important for understanding synaptic communication, yet it is incompletely understood, partly due to limited tools for assessing protein turnover *in vivo*. Here, we present ARGO (Analysis of Red-Green Offset), a fully genetically encoded, ratiometric fluorescence imaging method that visualizes and quantifies protein turnover with subcellular resolution *in vivo*. ARGO involves cell-specific labeling of the protein-of-interest with both RFP and GFP, followed by Cre/Lox-mediated removal of GFP (pulse) and periodic ratiometric imaging to track protein turnover (chase). This approach is inexpensive, modular, and scalable for use in genetically tractable experimental organisms. Using ARGO, we examined the turnover of Synaptogyrin/SNG-1, an evolutionarily conserved, integral SV protein, in adult *Caenorhabditis elegans* neurons. Our findings support the model that SV proteins are sorted for degradation at the synapse, then trafficked to the neuron cell body to complete degradation. We show that the rate of presynaptic SNG-1 turnover is consistent across synapses within a single neuron, indicating a cell-wide super-pool for SV protein degradation. Our results further suggest that, contrary to prevailing models, neither the surveillance nor the sorting of SV proteins for degradation is a rate-limiting step for SNG-1 turnover; rather, the rate-limiting step is the clearance of sorted-for-degradation SNG-1 from the presynapse.

Article Summary

How proteins are turned over within subcellular compartments is not well understood, in part because the phenomenon is difficult to quantify. The authors developed a simple, genetically encoded method to quantify the turnover of a protein-of-interest using fluorescence microscopy. They used this method to begin to assess synaptic vesicle protein turnover *in vivo*, as this is important for synaptic function. They found that synaptic vesicle protein Synaptogyrin/SNG-1 is sorted for degradation at the synapse but degraded in the neuron cell body, and the turnover rate depends on animal age but is constant across presynapses within a neuron.

Introduction

The maintenance of synaptic vesicle (SV) cycling throughout a neuron's extended lifespan requires SV protein turnover: the production and delivery of newly synthesized SV proteins balanced with the removal and degradation of damaged or excess SV proteins. The latter process – homeostatic protein degradation – remains incompletely understood, not only for SV proteins but also for most proteins in any cell type. An obstacle to understanding this is the lack of easy and robust methods to interrogate protein half-life *in vivo* with high spatial and temporal resolution.

Several methods can be used to quantify homeostatic protein turnover. Pulse-chase labeling with heavy-isotope-containing amino acids followed by bulk proteomics to measure reduction in labeled protein over time has the tremendous strength of simultaneously measuring the half-life of thousands of proteins (Zhou 2004). This method is laborious, though, especially *in vivo,* and the ability to measure protein half-life with cellular or subcellular resolution is limited since all of an animal's cells are labeled. A second method, arresting protein synthesis to measure reduction in total protein levels over time, can only be deployed in cultured cells for short time-windows due to the effects of arresting protein synthesis on cellular function and health (Zhou 2004). Fluorescence microscopy-based approaches enable assessment of an individual protein-of-interest's turnover with high resolution. This has been achieved using photoconvertible fluorescent proteins, which requires light access to the tissue of interest and careful calibration of the photoconversion to minimize phototoxicity in the "pulse" (Zhang et al. 2007). Another strategy is to label the protein-of-interest with a self-labeling tag, most commonly SNAP-tag or HaloTag, provide a "pulse" of fluorescent ligand, then image turnover with fluorescence microscopy during the "chase" (Bojkowska et al. 2011).

Importantly, comparing protein half-life between multiple separate studies that used the heavy-isotope-pulse-plus-proteomics approach shows that cultured neurons have dramatically shorter protein half-lives overall than neurons *in vivo* (Price et al. 2010; Cohen et al. 2013; Visscher et al. 2016; Dörrbaum et al. 2018; Fornasiero et al. 2018; Heo et al. 2018; Mathieson et al. 2018; Kluever et al. 2022). This indicates that there is a difference in the regulation of protein degradation in an adult animal's functioning nervous system verses in cultured neurons, highlighting the value of studying protein turnover *in vivo*.

Prior research mainly using assessment of steady-state SV protein localization combined with genetic analyses has led to the model that SV proteins are sorted into late endosomes and/or autophagosomes at the synapse, then transported to the cell body for degradation (Uytterhoeven et al. 2011; Fernandes et al. 2014; Sheehan et al. 2016; Okerlund et al. 2017). Both late endosomes and autophagosomes are found at presynapses based on electron microscopy and fluorescence-imaging approaches, but degradative lysosomes are predominantly located in the cell body and proximal neurites; to what extent they also found along axons and/or at presynpases remains a topic of debate (Winckler et

al. 2018; Farfel-Becker et al. 2019; Lie et al. 2021). SV proteins are not necessarily a cargo of presynaptic late endosomes or autophagosomes, however. This is because SVs are continuously trafficked between presynaptic terminals and throughout neurons, making an SV "super-pool" (Staras et al. 2010; Herzog et al. 2011; Wu et al. 2013). It is therefore possible that SV protein surveillance and sorting for degradation could happen entirely in the neuron cell body or some other location outside of the synapse. On the other hand, it has been suggested that SV protein degradation may be both initiated and completed in the axon during brain development in *D. melanogaster* (Jin et al. 2018). Another aspect under investigation is how the rate of SV protein degradation is regulated, with evidence pointing to both surveillance and/or sorting for degradation as rate-limiting steps (Fernandes et al. 2014; Sheehan et al. 2016; Okerlund et al. 2017; Sheehan and Waites 2019; Hoffmann-Conaway et al. 2020; Birdsall et al. 2022). Direct observation of SV protein turnover will potentiate a deeper understanding of this process.

Here, we developed a new method to visualize protein turnover with high spatial and temporal resolution *in vivo* using fluorescence microscopy. We call this method ARGO (Analysis of Red Green Offset), drawing an analogy to the Theseus Paradox, which ponders how identity persists as individual components are gradually replaced over time – a concept sometimes associated with the ship Argo. This method could, in theory, be applied to any protein-of-interest for which the addition of a fluorescent tag does not impact localization or function. Here, we use ARGO to analyze the turnover of Synaptogyrin/SNG-1, an evolutionarily conserved transmembrane SV protein that regulates SV cycling (Abraham et al. 2011; Raja et al. 2019). Our data support the model that SV proteins are sorted for degradation at the synapse and trafficked to the neuron cell body to complete degradation. They show that SNG-1 presynaptic turnover becomes slower in aging. They further show that SNG-1 turnover within a neuron is uniform across the presynapses, suggesting that SVs behave as a cell-wide super-pool in regard to SV protein degradation. Finally, they suggest that the rate-limiting step for degradation of this SV protein is neither surveillance nor sorting for degradation but rather the clearance of sorted-for-degradation SNG-1 from the presynapse.

Results

Generation and validation of SNG-1::ARGO

To enable the analysis of SNG-1 turnover with subcellular resolution *in vivo*, we developed the ARGO (Analysis of Red Green Offset) method (Fig 1). To summarize the ARGO method, the ARGO construct cell-specifically, co-translationally labels the protein-of-interest, in this case SNG-1, with both RFP and GFP in a tandem tag. Cell specificity is achieved using FLP/FRT, wherein the Flippase is expressed from neuron-specific promoters (Fig 1B). Assessing the steady-state GFP/RFP ratio of an

134 ARGO-tagged protein is informative for determining the mechanism of degradation: as GFP fluorescence
135 is quenched in acidic environments, ARGO-tagged proteins that have been sorted for degradation within
136 lysosomal compartments are detected as endosomes with stronger RFP fluorescence compared to GFP.
137 Alternatively, the absence of detectable lysosomal compartments suggests that the protein-of-interest is
138 degraded by the proteosome, or not at all. Next, a "pulse" removes *gfp* from the *argo* gene cassette such
139 that all newly produced molecules of the protein-of-interest are labeled with only RFP (Fig 1C). The neuron
140 is then periodically imaged with fluorescence microscopy, and the GFP/RFP ratio is quantified for each
141 fluorescent punctum throughout the cell to determine the proportion of "old" versus "total" protein-of-interest
142 both spatially and temporally.

143 The *argo* cassette was inserted into the *sng-1* genomic locus such that the RFP::GFP tandem tag
144 is attached to the C-terminus of SNG-1, which resides on the cytoplasmic side of SVs (Fig 1). Expression
145 of Flippase from a pan-neuronal reporter shows SNG-1::ARGO dually-labeled with RFP and GFP
146 fluorescence throughout the nervous system (Fig 2A-B). Using transgenes that drive Flippase expression
147 from neuron-specific promoters, we turned on SNG-1::ARGO expression in two specific neurons: the
148 cholinergic motor neuron DA9 (Fig 2C) and the serotonergic neuron NSM (Fig 2D). Both of these neurons
149 elaborates multiple *en passant* synapses that can be visualized as individual "puncta" using fluorescence
150 confocal microscopy (White et al. 1986). The use of neuron-specific Flippase transgenes enables
151 visualization of these individual presynapses, to which SNG-1::ARGO localizes as expected, with co-
152 localized fluorescence from RFP and GFP (Fig 2C-D)(Schwartz and Jorgensen 2016; Muñoz-Jiménez et
153 al. 2017). In the absence of a transgene expressing Flippase, no fluorescence is observed from the *sng-*
154 *1::argo* allele (Fig 2E).

155 For the ARGO method to provide biologically meaningful information about protein turnover, it must
156 not impact the function of the protein-of-interest. This is because each of the facets of a protein's function,
157 including folding, localization, and activity, are factors that could be inputs to regulate its turnover. For
158 SNG-1::ARGO, proper localization to the presynapses is the first indicator that this allele is useable. Next,
159 we assessed *sng-1* function. Synaptogyrin/SNG-1 regulates synaptic vesicle function from worms to
160 mammals (Abraham et al. 2011; Raja et al. 2019). In *C. elegans*, loss of *sng-1* leads to resistance to the
161 acetylcholinesterase inhibitor aldicarb, suggesting that the *sng-1(o)* mutant has reduced SV release
162 compared to wild-type (Fig 2F) (Mahoney et al. 2006; Abraham et al. 2011). By contrast, pan-neuronally
163 expressed SNG-1::ARGO has no discernable effect on aldicarb resistance compared to wild-type (Fig 2F),
164 indicating that the SNG-1::ARGO protein is functional. Together, these results suggest that SNG-1::ARGO
165 is a valid tool for investigating SNG-1 biology.

166 To generate the "pulse" that activates ARGO, we excised *gfp* from the *ARGO* gene cassette using
167 a heat-shock promoter to drive production of Cre recombinase upon a brief heat shock. This is the quickest

168 and most robust method to acutely induce gene expression in *C. elegans*. Indeed, we observed that this
169 method efficiently activated SNG-1::ARGO in both of the neurons we examined, with little ectopic excision
170 of *gfp* in the absence of heat shock (Table 1). The *sng-1::argo* showed maximal recombination of the
171 genomic locus by four hours after the initiation of the heat shock (Fig S1A). Though it is practical, a
172 drawback to this approach is that heat shock causes increased production of HSF-1-regulated genes
173 including chaperones, which will have some impact on proteostasis. To assess whether this is likely to
174 have a substantial impact on SNG-1 turnover dynamics or mechanisms, we assessed whether *sng-1*
175 mRNA or protein abundance are altered by the heat shock treatment. We reasoned that, if neither the rate
176 of SNG-1 production nor the steady-state abundance of SNG-1 is impacted by the heat shock, then it is
177 unlikely that the degradation is altered. Indeed, we observe no significant difference in *sng-1* mRNA levels
178 either 5 hours or 1 day after heat-shock (Fig S1B). To assess steady-state SNG-1 protein abundance, we
179 quantified average presynaptic SNG-1::ARGO RFP intensity and presynapse number in the DA9 neuron.
180 There was no significant difference in RFP intensity or synapse number 4 hours, 1 day, or 2 days after
181 heat shock (Fig S1C, D). Together, these data indicate that SNG-1::ARGO turnover is unlikely to be
182 substantially impacted by the heat shock "pulse." Any subtle impact is mitigated by the fact that all
183 comparisons of turnover are made between cohorts that received the same "pulse" treatment.
184

185 **SNG-1 is likely sorted for degradation at the presynapse and degraded in the cell body**

186 First, we assessed steady-state SNG-1::ARGO in greater detail. We noticed that, whereas the
187 presynaptic SNG-1::ARGO shows strong fluorescence from both the RFP and GFP, making the
188 presynapses appear white in the composite images, there are fluorescent puncta within the neuron cell
189 bodies that appear more red (Fig 2A-D). To quantify this, we measured the SNG-1::ARGO GFP/RFP ratio
190 at each presynapse and in each cell body punctum in the DA9 neuron in Day 2 adults. At the presynapses,
191 the DA9 neuron's average SNG-1::ARGO GFP/RFP steady-state ratio is 2.0, consistent with the fact that
192 GFP has a higher quantum yield than RFP and is consistently brighter *in vivo* (Rodriguez et al. 2017). In
193 the neuron cell body, however, the average GFP/RFP ratio of SNG-1::ARGO puncta is 1.0. The most
194 parsimonious explanation for this low GFP/RFP ratio is that these cell body puncta are acidic lysosomal
195 compartments to which SNG-1::ARGO has been sorted for degradation, and in which GFP fluorescence
196 is partially quenched due to its relatively high pKa. The NSM neuron in Day 2 adults shows a similar
197 difference between presynaptic versus cell body SNG-1::ARGO fluorescence. These data are consistent
198 with the model that at least some, and possibly all, of SNG-1 degradation occurs within endolysosomes
199 and/or autolysosomes within the neuron cell body.

200 Interestingly, the average steady-state SNG-1::ARGO GFP/RFP ratio at the presynapses between
201 the DA9 and NSM neurons is significantly different, at 2.0 (SD $\pm$ 0.2) and 1.6 (SD $\pm$ 0.3), respectively (Fig

202 2G). This suggests that A) a proportion of presynaptic SNG-1 resides within acidic compartments and B)
203 the steady-state proportion of presynaptic SNG-1 on SVs versus in acidic compartments varies by neuron
204 type: the NSM neuron has a higher proportion of presynaptic SNG-1 within acidic compartments compared
205 to the DA9 neuron. Consistent with this interpretation, late endosomes and autophagosomes, which both
206 have acidified lumens, localize to presynapses (Ceccarelli et al. 1973; LaVail and LaVail 1975; Grill et al.
207 2007; Binotti et al. 2015; Soukup et al. 2016; Stavoe et al. 2016; Neisch et al. 2017). To directly test this
208 interpretation, we injected Day 3 adults with Bafilomycin A (BafA), a V-ATPase inhibitor, and quantified
209 SNG-1::ARGO fluorescence at the DA9 synapses (Fig 2H). The BafA injection caused an increase in the
210 presynaptic SNG-1::ARGO GFP/RFP ratio, indicating that the GFP is intact on the presynaptic SNG-
211 1::ARGO but partially quenched within acidic compartments.
212

213 **A substantial proportion of presynaptic SNG-1 resides within acidic compartments by early**
214 **adulthood**

215 We continued our analysis of steady-state SNG-1::ARGO by quantifying presynaptic fluorescence
216 across early adulthood, from Day 0 - 7. Mean adult lifespan is ~15 days, so our imaging covered
217 approximately the first half of adult lifespan (Gems and Riddle 2000). We reasoned that the SNG-1::ARGO
218 RFP intensity is a readout for the total abundance of SNG-1 protein at the presynapse, as RFP intensity
219 from SV-localized SNG-1 versus SNG-1 residing within presynaptic acidic compartments will be similar.
220 On the other hand, the SNG-1::ARGO GFP intensity is a better indicator of the amount of SNG-1 on SVs,
221 the plasma membrane, or early endosomes, but not within acidic, pre-degradative compartments. As GFP
222 is only partially quenched in late endosomes or autophagosomes, the GFP intensity is an overestimate of
223 the pool of SNG-1 outside of acidic compartments.

224 In the DA9 neuron, the number of presynapses increases progressively from Day 0, imaged at the
225 L4 larval stage that precedes the final molt to adulthood, until Day 2, scaling with the overall growth of the
226 animal during this timeframe (Supplemental Fig 1C). The average SNG-1::ARGO RFP fluorescence
227 intensity per synapse increases from Day 0 to Day 2 of adulthood by over 100% (Fig. 3A, C). The average
228 SNG-1::ARGO GFP fluorescence intensity per synapse likewise increases, but by only half as much (Fig.
229 3B, C). In consequence, the average presynaptic SNG-1::ARGO GFP/RFP ratio decreases by about 25%
230 from Day 0 to Day 2. From Day 2 to Day 7 of adulthood, the SNG-1::ARGO fluorescence intensities are
231 fairly stable. These data suggest that the DA9 presynapse undergoes a change during early adulthood,
232 wherein a greater proportion of presynaptic SNG-1 has likely been sorted into pre-degradative
233 compartments by Day 2 compared to Day 0. Because GFP quenching is partial, it is unclear from these
234 data whether the abundance of SNG-1 on SVs also increases or whether the amount of SNG-1 functioning
235 in the SV cycle remains constant.

236 The data from the NSM neuron show a similar phenomenon as the DA9 neuron: both RFP and
237 GFP intensity from SNG-1::ARGO increases from Day 0 to Day 2 of adulthood, but RFP intensity increases
238 by about two times as much as GFP intensity (Fig. 2E-G). The SNG-1::ARGO GFP/RFP ratio declines for
239 a longer time period in the NSM neuron than in the DA9 neuron - from Day 0 to Day 5 of adulthood.
240 Considering that the SNG-1::ARGO un-quenched fluorescence intensity ratio is at least 2.4 (based on the
241 Day 0 DA9 measurement), our data suggest that more than 50% of presynaptic SNG-1 in the NSM neuron
242 resides within acidic compartments at Day 5 of adulthood.
243 Considering these data together, there is a general phenomenon that SNG-1 accumulates within
244 presynaptic acidic compartments, which are likely late endosomes and/or autophagosomes destined for
245 degradation, during early adulthood. The proportion of SNG-1 within these degradative compartments
246 versus in the SV pool, and the timing of this acidic compartment accumulation, depends on neuron identity
247 rather than being an intrinsic property of the SNG-1::ARGO protein or animal age.
248 In regard to the ARGO method, for both the DA9 and NSM neurons, the standard deviation between
249 animals for the raw fluorescence intensity values of SNG-1::ARGO RFP and GFP are larger than the
250 standard deviation in the GFP/RFP ratio. This is at least partially due to technical considerations, in that
251 as we are imaging neurons *in situ*, the fluorophore's fluorescence must pass through some animal tissue
252 including the cuticle. The fluorescence intensity detected is therefore highly dependent on animal position,
253 though we imaged animals in as uniform of positions as was practically feasible. This phenomenon is also
254 likely to have biological underpinnings, in that, though the *C. elegans* neural connectivity is invariant, the
255 precise position and size of each presynapse varies from animal to animal for all three of these neurons.
256 Both the technical and biological sources of variability is normalized by the ratiometric quantification of the
257 ARGO, highlighting the utility of this approach for high-resolution quantification.
258

259 **The rate of presynaptic SNG-1 turnover depends on animal age but not synapse position**

260 For turnover experiments using the SNG-1::ARGO, we first assessed the impact of aging on SNG-
261 1 presynaptic half-life. Using the DA9 neuron, we activated SNG-1::ARGO at Day 0, 2, 4, and 6 of
262 adulthood (Fig 4A-C). For each age, we imaged cohorts of animals daily for five days after activating the
263 SNG-1::ARGO, plus a cohort immediately before the pulse (Fig 4A-D). Fitting a single-phase exponential
264 decay function to each data set, we found that the apparent presynaptic half-life of SNG-1 at Day 0 of
265 adulthood is 1.6 days (95% C.I. 1.4 - 1.8 days). It increases between Day 0 to Day 2 of adulthood to 2.5
266 days (95% C.I. 2.3 - 2.8 days), and it is stable from Day 2 to Day 4. Between Day 4 to Day 6, it increases
267 to 3.9 days (95% C.I 3.2 - 4.7 days).
268 Considering, first, the difference between Day 0 and Day 2: the synapses grow by over 100%
269 between Day 0 to Day 2 (Fig 3A, C), and additional presynapses are added (Fig S1C), meaning that the

apparent half-life of SNG-1 at D0 measures a combination of both the removal of old molecules of SNG-1 from synapses and the increasing total abundance of SNG-1 at the presynapses. Further, steady-state GFP intensity declines during this period, likely due to increased sorting to acidic compartments for degradation. Starting at Day 2 of adulthood, the presynapse size (based on SNG-1::RFP intensity) and number, and the SNG-1::ARGO GFP/RFP ratio are stable (Fig 3A, 3C, S1C). This means that the declining SNG-1::ARGO GFP/RFP after activation is due to homeostatic SNG-1 turnover, wherein molecules of SNG-1::ARGO dually-labeled with both RFP and GFP are removed at the same rate as they are replaced by molecules of SNG-1::ARGO labeled with RFP only. The shorter apparent half-life at Day 0 compared to Day 2 is likely due to these factors.

Considering the slower presynaptic SNG-1 turnover at Day 6 of adulthood compared to Day 4: because the synapses are stable during this period, it is likely that this change is due to slowed degradation. This finding parallels the increase of average protein half-life with aging that has been reported based on several studies using pulse-chase heavy-isotope labeling (Depuydt et al. 2016; Visscher et al. 2016; Andrews et al. 2022; Kluever et al. 2022). It also corroborates our recent finding that aging leads to inadequate neuronal lysosomal function (Zhong et al., 2024).

Next, to compare SNG-1 turnover rate across different neurons, we activated the SNG-1::ARGO at Day 2 of adulthood in the DA9 versus the NSM neuron (Fig 4D-F). At this age, the synapses have mostly reached a phase of steady-state maintenance in regard to size and SNG-1::ARGO GFP/RFP ratio (Fig 3), meaning that the decrease in GFP/RFP ratio after ARGO activation is largely due to SNG-1 turnover. The apparent presynaptic half-life of SNG-1 is similar in the DA9 and NSM neurons (2.6 and 2.3 days, respectively) (Fig 4D-F). This result contrasts with that of the DA9 aging experiment in that here, the lower steady-state presynaptic GFP/RFP ratio in the NSM neuron compared to the DA9 neuron does not correspond to slower turnover.

To test the hypothesis that SV and/or degradative machinery trafficking might be rate-limiting for SV protein turnover, we quantified the apparent half-life of SNG-1::ARGO from the most proximal 10% and most distal 10% of presynapses. We detected no difference in the SNG-1 turnover rate based on presynapse position, indicating that the turnover rate of SNG-1 is likely regulated at the level of the whole neuron rather than at individual synapses, and that trafficking is not rate-limiting (Fig 4F).

Discussion

Here, we developed and validated ARGO, a genetically encoded method to easily and inexpensively quantify protein turnover *in vivo* with high spatial and temporal resolution. We used this

304 method to begin to assess how transmembrane SV protein Synaptogyrin/SNG-1 is turned over from the
305 presynapses. Our data indicate that SNG-1 is surveilled and sorted for degradation at the presynapse, and
306 a large proportion of presynaptic SNG-1 resides in acidic, likely sorted-for-degradation, compartments in
307 adulthood. The rate of SNG-1 turnover is constant across synapses within a neuron, and the steady-state
308 proportion of SNG-1 that has been sorted for degradation does not predict the turnover rate. We show
309 SNG-1 is degraded, at least in part, in the cell body, but trafficking is not limiting for degradation rate.
310 Finally, we show that presynaptic SNG-1 turnover slows with aging, and, as explained below, we propose
311 that this slowing is at least in part due to lysosome dysfunction. These findings provide new insights into
312 SV protein degradation, and they illustrate the utility of the ARGO method.
313

314 **The ARGO method**

315 The abundance of each of a cell's proteins is determined by its rates of production and degradation,
316 plus the rate of cell division (Liu et al. 2016). In terminally differentiated cells such as neurons, the protein
317 degradation rate takes a more prominent role in controlling protein abundance (Liu et al. 2016). Evidence
318 from proteomic studies indicates that protein half-life can range from minutes to months (and, rarely, even
319 longer), depending on the protein, the cell type, and the cellular context (Toyama et al. 2013). An
320 impediment to understanding the regulation of protein degradation is the limits of existing methods for
321 easily assessing protein degradation *in vivo* with high resolution. The most straight-forward existing
322 approach for interrogating a protein-of-interest's turnover is adding a self-labeling tag to that protein, most
323 commonly SNAP-tag or HaloTag, providing a "pulse" of fluorescent ligand, then imaging turnover with
324 fluorescence microscopy during the "chase" (Bojkowska et al. 2011; Bulovaite et al. 2022). ARGO is a
325 conceptually and methodologically similar strategy with several advantages: First, because ARGO is fully
326 genetically encoded, once the strain has been generated, performing experiments is simpler and cheaper.
327 This makes it highly amenable to thorough interrogation of surveillance and degradation mechanisms, for
328 example with forward and reverse genetics. Second, because the imaging is ratiometric, it provides higher
329 resolution of protein half-life, and it is advantageous to use with genetic or circumstantial manipulations
330 that alter the steady-state localization of the protein-of-interest. Third, because the GFP fluorescence is
331 sensitive to acidic environments, analysis of steady-state fluorescence can determine whether and where
332 degradation is mediated via sorting into a lysosomal pathway. The design of ARGO is modular, making it
333 amenable to modification. For instance, though we used heat shock promoter to drive Cre expression here,
334 any temporally inducible transcription system can, in theory, be used to provide the "pulse."
335

336 **SV protein degradation**

337 The degradation of SV proteins, and by extension, SVs, is a key parameter for controlling synaptic
338 function, yet it remains incompletely understood. Our data indicate that SNG-1 is sorted for degradation at
339 the synapse, then transported to the cell body for degradation in lysosomal compartments. This
340 corroborates the most prevailing, though sometimes disputed, model for the spatial dynamics of SV protein
341 degradation (Jin et al. 2018; Winckler et al. 2018). We show that SNG-1 half-life increases in mid adulthood
342 compared to younger adulthood. This aligns with prior work showing that protein turnover generally slows
343 with aging from worms to mammals (Depuydt et al. 2016; Visscher et al. 2016; Andrews et al. 2022; Kluever
344 et al. 2022). Indeed, accumulation of damaged or misfolded proteins, due at least in part to ineffective
345 protein surveillance and/or degradation, is a hallmark of aging (López-Otín et al. 2023).
346 We show that presynaptic SNG-1 turnover within a neuron does not depend on presynapse position
347 (Fig 4F). This suggests that the cell's SNG-1, and by extension, its SVs, function as a single super-pool in
348 regard to turnover. This contrasts with post-synaptic protein PSD95, for which the turnover rate differs
349 between post-synapses within a single neuron based on their spatial positioning in the mouse brain
350 (Bulovaite et al. 2022), and it points to the dynamic and continuous trafficking of SVs between synapses
351 (Staras et al. 2010; Herzog et al. 2011; Wu et al. 2013). It also indicates that trafficking is not rate-limiting
352 for SV protein turnover.
353 Quantification of the steady-state SNG-1::ARGO GFP/RFP ratio suggests that a large proportion
354 of presynaptic SNG-1 resides in acidic compartments that are likely late endosomes and/or autophagomes
355 – greater than 50% in the NSM neuron in adult animals (Fig 3). The prevailing understanding would say
356 that these SNG-1 proteins have been decommissioned and sorted for degradation. Though this may seem
357 unlikely at face value, it aligns well with evidence from cultured hippocampal neurons indicating that SV
358 proteins function in SV cycling for less than half of their total half-life, and, once decommissioned from SV
359 cycling, they continue to reside at presynapse (Truckenbrodt et al. 2018). On the other hand, sorting to
360 acidic endosomal compartments may not represent an irrevocable exit from the SV cycle – intraluminal
361 vesicles within late endosomes can undergo back-fusion/retrofusion, allowing resident proteins to re-join
362 the functional pool (Eden and Futter 2021; Perrin et al. 2021). It will be interesting to distinguish between
363 these two possibilities in future studies.
364 Whether or not the presynaptic SNG-1 within acidic compartments has been fully decommissioned
365 from the SV cycle, it is expected to have passed the initial surveillance and sorting checkpoints for
366 degradation. This suggests that surveillance and sorting are not rate-limiting for SV protein degradation,
367 in contrast to prevailing models (Uytterhoeven et al. 2011; Fernandes et al. 2014; Sheehan et al. 2016;
368 Birdsall et al. 2022). Instead, the clearance of sorted-for-degradation SNG-1 from the presynapse is rate-
369 limiting. We speculate that this clearance from the presynapse is regulated by lysosome function, at least
370 during aging, based on two lines of evidence: First, aging leads to slowed presynaptic SNG-1::ARGO

371 turnover (Fig 4A-B), and our recent findings showed that neuronal lysosomal function declines with aging
372 along a similar timeline (Zhong et al., 2024). Second, our recent work indicates that reducing neuronal
373 lysosomal capacity via loss-of-function of lysosome biogenesis effector Transcription Factor EB
374 (TFEB)/HLH-30 leads to slowed SNG-1::ARGO presynaptic turnover (Zhong et al., 2024).
375
376
377

378 Materials and Methods

379 *C. elegans* culture and maintenance

380 Nematodes were grown at room temperature on nematode growth media (NGM) plates seeded with
381 *Escherichia coli* OP50. All experiments used hermaphrodite worms and the stages used for each
382 experiment are outlined in the figure legends. Several strains were provided by the Caenorhabditis
383 Genetics Center (CGC), which is funded by NIH Office of Research Infrastructure Program (P40
384 OD010440). The *carIs1(Pglr-4>Flippase)* allele, which flips-on *sng-1::argo* in the DA9 neuron, was
385 generated by integrating *shyEx246* from the Shaul Yogev lab. To induce expression of *Pheat-*
386 *shock>Cre(heSi160)* for ARGO activation, worm plates were sifted to a 34 °C incubator for one hour.
387 Strains used in this study: PBT68 *bqSi506(Prgef-1>Flp, unc-119(+)) IV; sng-1(syb3140car2) heSi160 X*,
388 PBT67 *carIs1(Pglr-4>Flp, Podr-1>rfp) II; sng-1(syb3140car2) heSi160 X*, PBT188 *bqSi488(Ptph-1>Flp,*
389 *unc-119(+) IV; sng-1(syb3140car2) heSi160 X*, PBT84 *sng-1(syb3140car2), RB503 sng-1(ok234) X*,
390 PBT58 *bqSi542(Punc-47>Flp, unc-119(+) IV; sng-1(syb3140) heSi160 X*.
391

392 Genome editing using CRISPR/Cas9

393 An initial ARGO allele, *sng-1(syb3140)*, consisting of *FRT-stop+3'utr-FRT-RFP-loxP-GFP-loxP,* was
394 generated by SunyBiotech. We determined that the resulting SNG-1::RFP::GFP causes SNG-1
395 destabilization and accelerated degradation. Removal of GFP upon ARGO activation led to increased RFP
396 fluorescence intensity up to the expected intensity based on existing strains (Schwartz and Jorgensen
397 2016), indicating that the amino acid linker between the RFP and GFP was causing the destabilization.
398 We therefore used CRISPR/Cas9 to modify the amino acid linker between the RFP and GFP in the *sng-*
399 *1(syb3140)* allele, generating the *sng-1(syb3140car2)* allele. This fixed the destabilization issue and was
400 used in all experiments in this study except for Fig S1A, which quantifies the rate of Cre-mediated
401 recombination, which is expected to be identical between *syb3140* and *syb3140car2*. The *car2* allele was
402 generated following the protocol in (Paix et al. 2015). A ssDNA with 36 and 38 bp homology on either side
403 was used for the repair template (Ultramer, Integrated DNA Technologies (IDT). Two cRNAs (IDT) were

404 used, one on either end of the edit. The genomic sequence of the *argo* cassette and the cDNA sequences
405 of *sng-1::argo* before and after the removal of *GFP* are provided Supplementary Figs 2-4.
406

407 ## Aldicarb assay

408 Aldicarb assays were performed as described (Mahoney et al., 2006). Briefly, 30 Day 1 adults of each
409 strain were placed on a plate containing 0.5 mM aldicarb, and they were periodically assessed for paralysis
410 visually after touch with an eyelash. Plates were scored blind to genotype, and the experiment was
411 executed in three biological replicates, each on a separate day.
412

413 **qPCR of genomic DNA**

414 Day 0/L4 animals of the genotype *bqSi542; sng-1(syb3140) heSi160* were shifted to 34 °C for 1 hour at
415 Time = 0. Directly before the shift, and at the indicated times afterward, approximately 50 animals were
416 picked and lysed with the standard worm lysis protocol. Relative abundance of the Cre-recombined locus
417 was assess using primers that aligned to the 3' end of *RFP* before the first *loxP* and the 3' end of *sng-1*
418 after the second *loxP.* Relative transcript abundance was calculated using the ΔΔCt method, with primers
419 against *gpi-1* used as the internal control. All reactions were performed in triplicate.
420

421 ## RNA extraction and qPCR

422 Total RNA was extracted from *Caenorhabditis elegans* samples using the TRI reagent (Sigma Aldrich),
423 ethanol precipitation protocol. The LunaScript Kit (NEB) was used for complementary DNA (cDNA)
424 synthesis according to the manufacturer's protocol. Quantitative RT-PCR was performed using the Roche
425 Lightcycler 480. Primers for the target genes (*sng-1, hsp-16*) and the reference/normalization gene (*pmp-*
426 *42*) were validated empirically for specificity and efficiency. Melting curve analysis was performed at the
427 end of each run to confirm amplification specificity. Gene expression levels were calculated using the ΔΔCt
428 method, with the *pmp-42* gene serving as the internal control. All reactions were performed in triplicate.
429

430 ## Microscopy and imaging

431 Worms were mounted on 3% freshly made agarose pads into drops of 20 mM levamisole. An imaging
432 system comprised of a Nikon Eclipse Ti2 microscope, Yokogawa CSU-W1 SoRa spinning-disk unit and a
433 Hamamatsu ORCA-fusionBT digital camera C15440 with Plan Apo x60 A1/2 Nikon objective with water
434 immersion was used to acquire all images. Image settings (60% of laser power and 200 ms exposure time)
435 were identical for all groups and treatments across experiments. Z-stacks were taken with 0.4 µm step in
436 the 20-30 µm range, depending on type of neuron.
437

438 **Data Analysis**

439 Nd2 files were screened with NIS Elements Software for unusually low signal, severe movement or drifting
440 and discarded, the rest images were processed with Fiji (ImageJ) software. Image stacks were transformed
441 using z-projection function with max intensity option, areas of interest were selected either with Rectangle
442 tool (for cell bodies) or Segmented line and Straighten function (for synaptic areas). For each image, a
443 Threshold was applied with default settings to the RFP channel, and the Analyze Particles function was
444 used to identify ROIs. These ROIs were then used to quantify fluorescence from both the RFP and GFP
445 channels. Each obtained array of values in csv format was united in a single data frame, synaptic puncta
446 less than 0.3 μm^2 were filtered out due to high variability in relative RFP:GFP fluorescence intensities, and
447 the GFP/RFP ratio calculation was done with Jupyter Notebook and Python scripts. Prism GraphPad
448 software was used to generate plots and perform statistical analyses. SNG-1::ARGO half-life was
449 calculated using Prism to fit one phase exponential decay curves, constraining the plateau to the
450 experimentally determined value based on background GFP fluorescence, which comes from
451 autofluorescence. The curves were fitted using least squares regression with no weighting, and outliers
452 were detected and eliminated with Q = 1%. Comparisons of half-life between curves was performed using
453 Extra sum-of-squares F test.

454

455 **Bafilomycin A treatment**

456 Bafilomycin A was injected into the body cavity of *C. elegans* similarly to previous work (Wilkinson et al.,
457 2015). Briefly, 25 μM of BafA in 0.2% DMSO or 0.2% DMSO ("mock") was co-injected with Orange G for
458 color into the pseudocoelom, and animals were allowed to recover for three hours before they were imaged
459 with fluorescence confocal microscopy as described above. BafA injected animals were still moving when
460 they were put on slides, indicating that the BafA had not completely blocked V-ATPase function.

461

462

463 ## Acknowledgments

464 Some strains were provided by the Caenorhabditis elegans Genetics Center (CGC), which is funded by
465 the National Institutes of Health (NIH) Office of Research Infrastructure Programs (P40 OD010440). The
466 Shaul Yogev lab provided *shyEx246*, which was integrated to generate *carIs1*. We thank Julianna Miller,
467 Emma Keep, Adam Darlington, Margaret Brener, and Sophia Whitley for assistance in the lab.

468 ## Funding

469 This work was supported by the National Institutes of Health (NIH) grant R35 GM154869 to C.E.R.

References

Abraham C, Bai L, Leube RE. 2011. Synaptogyrin-dependent modulation of synaptic neurotransmission in *Caenorhabditis elegans*. Neuroscience. 190:75–88. doi:10.1016/J.NEUROSCIENCE.2011.05.069.

Andrews B, Murphy AE, Stofella M, Maslen S, Almeida-Souza L, Skehel JM, Skene NG, Sobott F, Frank RAW. 2022. Multidimensional Dynamics of the Proteome in the Neurodegenerative and Aging Mammalian Brain. Mol Cell Proteomics. 21(2):100192. doi:10.1016/J.MCPRO.2021.100192.

Binotti B, Pavlos NJ, Riedel D, Wenzel D, Vorbrüggen G, Schalk AM, Kühnel K, Boyken J, Erck C, Martens H, et al. 2015. The GTPase Rab26 links synaptic vesicles to the autophagy pathway. Elife. 4. doi:10.7554/elife.05597.

Birdsall V, Kirwan K, Zhu M, Imoto Y, Wilson SM, Watanabe S, Waites CL. 2022. Axonal transport of Hrs is activity dependent and facilitates synaptic vesicle protein degradation. Life Sci Alliance. 5(10). doi:10.26508/LSA.202000745.

Bojkowska K, Santoni De Sio F, Barde I, Offner S, Verp S, Heinis C, Johnsson K, Trono D. 2011. Measuring in vivo protein half-life. Chem Biol. 18(6):805–815. doi:10.1016/J.CHEMBIOL.2011.03.014.

Bulovaite E, Qiu Z, Kratschke M, Zgraj A, Fricker DG, Tuck EJ, Gokhale R, Koniaris B, Jami SA, Merino-Serrais P, et al. 2022. A brain atlas of synapse protein lifetime across the mouse lifespan. Neuron. 110(24):4057-4073.e8. doi:10.1016/J.NEURON.2022.09.009.

Ceccarelli B, Hurlbut WP, Mauro A. 1973. Turnover of transmitter and synaptic vesicles at the frog neuromuscular junction. Journal of Cell Biology. 57(2):499–524. doi:10.1083/JCB.57.2.499.

Cohen LD, Zuchman R, Sorokina O, Müller A, Dieterich DC, Armstrong JD, Ziv T, Ziv NE. 2013. Metabolic Turnover of Synaptic Proteins: Kinetics, Interdependencies and Implications for Synaptic Maintenance. Akaaboune M, editor. PLoS One. 8(5):e63191. doi:10.1371/journal.pone.0063191.

Depuydt G, Shanmugam N, Rasulova M, Dhondt I, Braeckman BP. 2016. Increased Protein Stability and Decreased Protein Turnover in the *Caenorhabditis elegans* Ins/IGF-1 daf-2 Mutant. J Gerontol A Biol Sci Med Sci. 71(12):1553. doi:10.1093/GERONA/GLV221.

Dörrbaum AR, Kochen L, Langer JD, Schuman EM. 2018. Local and global influences on protein turnover in neurons and glia. Elife. 7. doi:10.7554/ELIFE.34202.

Eden ER, Futter CE. 2021. Membrane trafficking: Retrofusion as an escape route out of the endosome. Current Biology. 31(17):R1037–R1040. doi:10.1016/J.CUB.2021.07.055.

Farfel-Becker T, Roney JC, Cheng XT, Li S, Cuddy SR, Sheng ZH. 2019. Neuronal Soma-Derived Degradative Lysosomes Are Continuously Delivered to Distal Axons to Maintain Local Degradation Capacity. Cell Rep. 28(1):51-64.e4. doi:10.1016/J.CELREP.2019.06.013.

514 Farías GG, Guardia CM, De Pace R, Britt DJ, Bonifacino JS. 2017. BORC/kinesin-1 ensemble drives
515 polarized transport of lysosomes into the axon. Proc Natl Acad Sci U S A. 114(14):E2955–E2964.
516 doi:10.1073/PNAS.1616363114.
517
518 Fernandes AC, Uytterhoeven V, Kuenen S, Wang YC, Slabbaert JR, Swerts J, Kasprowicz J, Aerts S,
519 Verstreken P. 2014. Reduced synaptic vesicle protein degradation at lysosomes curbs TBC1D24/sky-
520 induced neurodegeneration. Journal of Cell Biology. 207(4):453–462. doi:10.1083/jcb.201406026.
521
522 Fornasiero EF, Mandad S, Wildhagen H, Alevra M, Rammner B, Keihani S, Opazo F, Urban I, Ischebeck
523 T, Sakib MS, et al. 2018. Precisely measured protein lifetimes in the mouse brain reveal differences across
524 tissues and subcellular fractions. Nature Communications 2018 9:1. 9(1):1–17. doi:10.1038/s41467-018-
525 06519-0.
526
527 Gems D, Riddle DL. 2000. Defining Wild-Type Life Span in Caenorhabditis elegans. The Journals of
528 Gerontology: Series A. 55(5):B215–B219. doi:10.1093/GERONA/55.5.B215.
529
530 Grill B, Bienvenut W V., Brown HM, Ackley BD, Quadroni M, Jin Y. 2007. C. elegans RPM-1 Regulates
531 Axon Termination and Synaptogenesis through the Rab GEF GLO-4 and the Rab GTPase GLO-1. Neuron.
532 55(4):587–601. doi:10.1016/J.NEURON.2007.07.009.
533
534 Heo S, Diering GH, Na CH, Nirujogi RS, Bachman JL, Pandey A, Huganir RL. 2018. Identification of long-
535 lived synaptic proteins by proteomic analysis of synaptosome protein turnover. Proc Natl Acad Sci U S A.
536 115(16):E3827–E3836. doi:10.1073/pnas.1720956115.
537
538 Herzog E, Nadrigny F, Silm K, Biesemann C, Helling I, Bersot T, Steffens H, Schwartzmann R, Valentin
539 Nägerl U, El Mestikawy S, et al. 2011. In vivo imaging of intersynaptic vesicle exchange using
540 VGLUT1Venus knock-in mice. Journal of Neuroscience. 31(43):15544–15559.
541 doi:10.1523/JNEUROSCI.2073-11.2011.
542
543 Hoffmann-Conaway S, Brockmann MM, Schneider K, Annamneedi A, Rahman KA, Bruns C, Textoris-
544 Taube K, Trimbuch T, Smalla KH, Rosenmund C, et al. 2020. Parkin contributes to synaptic vesicle
545 autophagy in bassoon-deficient mice. Elife. 9:1–30. doi:10.7554/ELIFE.56590.
546
547 Jin EJ, Kiral FR, Ozel MN, Burchardt LS, Osterland M, Epstein D, Wolfenberg H, Prohaska S, Hiesinger
548 PR. 2018. Live Observation of Two Parallel Membrane Degradation Pathways at Axon Terminals. Curr
549 Biol. 28(7):1027-1038.e4. doi:10.1016/j.cub.2018.02.032.
550
551 Kluever V, Russo B, Mandad S, Kumar NH, Alevra M, Ori A, Rizzoli SO, Urlaub H, Schneider A, Fornasiero
552 EF. 2022. Protein lifetimes in aged brains reveal a proteostatic adaptation linking physiological aging to
553 neurodegeneration. Sci Adv. 8(20):4437. doi:10.1126/SCIADV.ABN4437.
554
555 LaVail MM, LaVail JH. 1975. Retrograde intraaxonal transport of horseradish peroxidase in retinal ganglion
556 cells of the chick. Brain Res. 85(2):273–280. doi:10.1016/0006-8993(75)90081-5.
557

558 Lie PPY, Yang DS, Stavrides P, Goulbourne CN, Zheng P, Mohan PS, Cataldo AM, Nixon RA. 2021. Post-
559 Golgi carriers, not lysosomes, confer lysosomal properties to pre-degradative organelles in normal and
560 dystrophic axons. Cell Rep. 35(4). doi:10.1016/J.CELREP.2021.109034.
561
562 Liu Y, Beyer A, Aebersold R. 2016. On the Dependency of Cellular Protein Levels on mRNA Abundance.
563 Cell. 165(3):535–550. doi:10.1016/J.CELL.2016.03.014.
564
565 López-Otín C, Blasco MA, Partridge L, Serrano M, Kroemer G. 2023. Hallmarks of aging: An expanding
566 universe. Cell. 186(2):243–278. doi:10.1016/J.CELL.2022.11.001.
567
568 Mahoney TR, Luo S, Nonet ML. 2006. Analysis of synaptic transmission in *Caenorhabditis elegans* using
569 an aldicarb-sensitivity assay. Nature Protocols 2006 1:4. 1(4):1772–1777. doi:10.1038/nprot.2006.281.
570
571 Mathieson T, Franken H, Kosinski J, Kurzawa N, Zinn N, Sweetman G, Poeckel D, Ratnu VS, Schramm
572 M, Becher I, et al. 2018. Systematic analysis of protein turnover in primary cells. Nature Communications
573 2018 9:1. 9(1):1–10. doi:10.1038/s41467-018-03106-1.
574
575 Muñoz-Jiménez C, Ayuso C, Dobrzynska A, Torres-Mendéz A, Ruiz PDLC, Askjaer P. 2017. An efficient
576 flp-based toolkit for spatiotemporal control of gene expression in *Caenorhabditis elegans*. Genetics.
577 206(4):1763–1778. doi:10.1534/GENETICS.117.201012.
578
579 Neisch AL, Neufeld TP, Hays TS. 2017. A STR IPAK complex mediates axonal transport of
580 autophagosomes and dense core vesicles through PP2A regulation. Journal of Cell Biology. 216(2):441–
581 461. doi:10.1083/JCB.201606082.
582
583 Okerlund ND, Schneider K, Leal-Ortiz S, Montenegro-Venegas C, Kim SA, Garner LC, Gundelfinger ED,
584 Reimer RJ, Garner CC. 2017. Bassoon Controls Presynaptic Autophagy through Atg5. Neuron. 93(4):897-
585 913.e7. doi:10.1016/J.NEURON.2017.01.026.
586
587 Paix A, Folkmann A, Rasoloson D, Seydoux G. 2015. High efficiency, homology-directed genome editing
588 in *Caenorhabditis elegans* using CRISPR-Cas9 ribonucleoprotein complexes. Genetics. 201(1):47–54.
589 doi:10.1534/GENETICS.115.179382.
590
591 Perrin P, Janssen L, Janssen H, van den Broek B, Voortman LM, van Elsland D, Berlin I, Neefjes J. 2021.
592 Retrofusion of intralumenal MVB membranes parallels viral infection and coexists with exosome release.
593 Current Biology. 31(17):3884. doi:10.1016/J.CUB.2021.06.022.
594
595 Price JC, Guan S, Burlingame A, Prusiner SB, Ghaemmaghami S. 2010. Analysis of proteome dynamics
596 in the mouse brain. Proc Natl Acad Sci U S A. 107(32):14508–14513. doi:10.1073/PNAS.1006551107.
597
598 Raja MK, Preobraschenski J, Olmo-Cabrera S Del, Martinez-Turrillas R, Jahn R, Perez-Otano I, Wesseling
599 JF. 2019. Elevated synaptic vesicle release probability in synaptophysin/gyrin family quadruple knockouts.
600 Elife. 8. doi:10.7554/ELIFE.40744.
601

602 Rodriguez EA, Campbell RE, Lin JY, Lin MZ, Miyawaki A, Palmer AE, Shu X, Zhang J, Tsien RY. 2017.
603 The growing and glowing toolbox of fluorescent and photoactive proteins. Trends Biochem Sci. 42(2):111–
604 129. doi:10.1016/J.TIBS.2016.09.010.
605
606 Schwartz ML, Jorgensen EM. 2016. SapTrap, a toolkit for high-throughput CRISPR/Cas9 gene
607 modification in *Caenorhabditis elegans*. Genetics. 202(4):1277–1288.
608 doi:10.1534/GENETICS.115.184275.
609
610 Sheehan P, Waites CL. 2019. Coordination of synaptic vesicle trafficking and turnover by the Rab35
611 signaling network. Small GTPases. 10(1):54–63. doi:10.1080/21541248.2016.1270392.
612
613 Sheehan P, Zhu M, Beskow A, Vollmer C, Waites CL. 2016. Activity-dependent degradation of synaptic
614 vesicle proteins requires Rab35 and the ESCRT pathway. Journal of Neuroscience. 36(33):8668–8686.
615 doi:10.1523/JNEUROSCI.0725-16.2016.
616
617 Soukup SF, Kuenen S, Vanhauwaert R, Manetsberger J, Hernández-Díaz S, Swerts J, Schoovaerts N,
618 Vilain S, Gounko N V., Vints K, et al. 2016. A LRRK2-Dependent EndophilinA Phosphoswitch Is Critical
619 for Macroautophagy at Presynaptic Terminals. Neuron. 92(4):829–844.
620 doi:10.1016/J.NEURON.2016.09.037.
621
622 Staras K, Branco T, Burden JJ, Pozo K, Darcy K, Marra V, Ratnayaka A, Goda Y. 2010. A vesicle superpool
623 spans multiple presynaptic terminals in hippocampal neurons. Neuron. 66(1):37–44.
624 doi:10.1016/J.NEURON.2010.03.020.
625
626 Stavoe AKH, Hill SE, Hall DH, Colón-Ramos DA. 2016. KIF1A/UNC-104 Transports ATG-9 to Regulate
627 Neurodevelopment and Autophagy at Synapses. Dev Cell. 38(2):171–185.
628 doi:10.1016/J.DEVCEL.2016.06.012.
629
630 Toyama BH, Savas JN, Park SK, Harris MS, Ingolia NT, Yates JR, Hetzer MW. 2013. Identification of long-
631 lived proteins reveals exceptional stability of essential cellular structures. Cell. 154(5).
632 doi:10.1016/J.CELL.2013.07.037.
633
634 Truckenbrodt S, Viplav A, Jähne S, Vogts A, Denker A, Wildhagen H, Fornasiero EF, Rizzoli SO. 2018.
635 Newly produced synaptic vesicle proteins are preferentially used in synaptic transmission. EMBO J. 37(15).
636 doi:10.15252/EMBJ.201798044.
637
638 Uytterhoeven V, Kuenen S, Kasprowicz J, Miskiewicz K, Verstreken P. 2011. Loss of Skywalker reveals
639 synaptic endosomes as sorting stations for synaptic vesicle proteins. Cell. 145(1):117–132.
640 doi:10.1016/j.cell.2011.02.039.
641
642 Visscher M, De Henau S, Wildschut MHE, van Es RM, Dhondt I, Michels H, Kemmeren P, Nollen EA,
643 Braeckman BP, Burgering BMT, et al. 2016. Proteome-wide changes in protein turnover rates in
644 *C. elegans* models of longevity and age-related disease. Cell Rep. 16(11):3041–3051.
645 doi:10.1016/J.CELREP.2016.08.025.

White JG, Southgate E, Thomson JN, Brenner S. 1986. The structure of the nervous system of the nematode *Caenorhabditis elegans*. Philos Trans R Soc Lond B Biol Sci. 314(1165):1–340. doi:10.1098/RSTB.1986.0056.

Wilkinson DS, Jariwala JS, Anderson E, Mitra K, Meisenhelder J, Chang JT, Ideker T, Hunter T, Nizet V, Dillin A, Hansen M. 2015. Phosphorylation of LC3 by the Hippo kinases STK3/STK4 is essential for autophagy. Mol Cell 57(1): 55-68. doi:10.1016/j/molcel.2014.11.019.

Winckler B, Faundez V, Maday S, Cai Q, Guimas Almeida C, Zhang H. 2018. The Endolysosomal System and Proteostasis: From Development to Degeneration. J Neurosci. 38(44):9364–9374. doi:10.1523/JNEUROSCI.1665-18.2018.

Wu YE, Huo L, Maeder CI, Feng W, Shen K. 2013. The balance between capture and dissociation of presynaptic proteins controls the spatial distribution of synapses. Neuron. 78(6):994–1011. doi:10.1016/J.NEURON.2013.04.035.

Zhang L, Gurskaya NG, Merzlyak EM, Staroverov DB, Mudrik NN, Samarkina ON, Vinokurov LM, Lukyanov S, Lukyanov KA. 2007. Method for real-time monitoring of protein degradation at the single cell level. Biotechniques. 42(4):446–450. doi:10.2144/000112453.

Zhong R, Richardson CE. 2024. TFEB/HLH-30-mediated expansion of neuronal lysosomal capacity in early adulthood protects dendrite maintenance during aging in *Caenorhabditis elegans.* BioRxiv doi: 10.1101/2024.11.29.625995.

Zhou P. 2004. Determining protein half-lives. Methods Mol Biol. 284:67–77. doi:10.1385/1-59259-816-1:067.

677

Table 1. Specificity and Efficacy of SNG-1::ARGO Activation by Heat-shock-Promoter driving *Cre* recombinase.

Specificity		
Neuron	**Age scored (d of adulthood)**	**GFP not recombined without heat shock (n)**
DA9	>= 4	95% (146)
NSM	>=6	100% (43)
Efficacy		
Neuron	**Age heat-shocked (d of adulthood)**	**GFP recombined after heat-shock (n)**
DA9	0	97.3% (108)
DA9	2	94% (65)
NSM	2	100% (55)

Parameters were assessed in strains carrying *sng-1::argo,* each individual neuron-specific flippase, and an integrated transgene composed of heat-shock promoter driving *Cre* recombinase (*heSi160*). Specificity means how often the *GFP* was not excised in the absence of heat-shock, and Efficacy means how often the *GFP* was excised upon heat-shock of 1 h at 34 ºC, scored based on visualizing SNG-1::ARGO GFP and RFP fluorescence at least 3 d after activation.

678

679

680

681 ## Figure captions

682 **Figure 1. Design of the ARGO method.** (a) (left) The *argo* gene cassette is inserted into the *gene-of-*
683 *interest*, ideally at the endogenous genomic locus. The strain also contains transgenes encoding neuron-
684 specific FLP-Flippase and a mechanism for inducible *Cre* expression. In this case, we tagged *sng-1* at the
685 genomic locus and used a heat-shock promoter to induce *Cre* expression. (right) The protein-of-interest,
686 in this case SNG-1, will be expressed with a short additional amino acid tag, which is encoded by the first
687 FRT sequence, in every cell. (b) Neuron-specific promoter drives *Flp* expression shortly after neuron birth.
688 These cells "turn on" the ARGO tag. (c) (left) A pulse of *Cre* expression removes *gfp* from the *argo* gene
689 cassette. (right) All newly synthesized SNG-1 will be tagged with RFP. Therefore, RFP fluorescence
690 reports total SNG-1 protein, whereas GFP reports "old" SNG-1.

691

692

693 **Figure 2. Steady-state SNG-1::ARGO fluorescence indicates that SNG-1 is largely degraded in the**
694 **cell body.** (a-b) Representative image of the head of an animal with the *sng-1::argo* allele in which the
695 ARGO tag is flipped-on by a pan-neuronally expressed Flippase, showing co-localized RFP and GFP

696 fluorescence at presynapses throughout the nervous system. (b) Zoomed-in view of the boxed area from
697 (a) showing a region where neuron cell bodies reside. Arrows point to endosomes with relatively brighter
698 RFP vs GFP intensity. (c-d) SNG-1::ARGO Flipped-on in individual neurons. Cartoons show neuron
699 morphology (blue) within the animal (black). In (c), red box shows where presynapses are located; the
700 NSM neuron (d) makes synapses throughout the neurites diagrammed. (e) In the absence of Flippase
701 expression, there is no detectable SNG-1::ARGO fluorescence. Blue dashed line outlines the head of the
702 animal. Scale = 10 um. (f) Sensitivity to 0.5 mM aldicarb in d1 adults (*P<0.05, **P<0.01, Chi-squared test
703 with Bonferroni correction, n = 90 animals per genotype, summed across three separate experiments). (g)
704 Quantification of SNG-1::ARGO GFP/RFP intensity from individual presynapses versus endosomes in the
705 neuron cell body in Day 2 adults. Bar shows mean ± SEM (ns: not significant, P>0.5. ****P<0.0001, one-
706 way ANOVA with Tukey post-test). (h) Presynaptic SNG-1::ARGO GFP/RFP intensity in the DA9 neuron
707 in Day 3 adults, control animals versus animals that were injected with a solution containing Bafilomycin A
708 ("BafA") or not ("mock"). Each data point is the average GFP/RFP from all presynapses within a single
709 neuron, within a single animal. Bar shows mean ± SEM (ns: not significant, P>0.5. **P<0.01, one-way
710 ANOVA with Sidak post-test).
711
712
713 **Figure 3. Presynaptic SNG-1::ARGO shows declining steady-state GFP/RFP fluorescence,**
714 **indicative of accumulation within acidic compartments, during early adulthood.** (a-b, e-f) Average
715 presynaptic intensity of RFP (a, e) and GFP (b, f) from SNG-1::ARGO expressed in the DA9 neuron (a-b)
716 and the NSM neuron (e-f). Each data point shows the average intensity of all presynapses from a single
717 neuron. (c, g) Percent change in average presynaptic RFP and GFP intensity from Day 0 of adulthood (L4
718 larval stage) through Day 2 of adulthood in DA9 (c) and NSM (g). Plotted is mean ± SEM of 10-17 animals
719 per neuron and time-point. (d, h) Average presynaptic SNG-1::ARGO GFP/RFP steady-state ratio in DA9
720 (d) and NSM (h). Bar shows mean ± SEM (ns: not significant, P>0.5. *P<0.05, **P<0.01, ***P<0.001,
721 ****P<0.0001, one-way ANOVA (a-b, d, e-f, h) or two-way ANOVA (c, g) with Tukey post-test).
722
723
724 **Figure 4. Presynaptic SNG-1 turnover rate depends on animal age but not subcellular position of**
725 **the synapse.** (a) Example images of SNG-1::ARGO in DA9 presynapses from an experiment in which the
726 SNG-1::ARGO was activated at Day 2 of adulthood, showing proximal synapses from three animals per
727 time-point. Scale = 30 µm. (b, d, e) SNG-1::ARGO turnover experiments in the DA9 neuron started at Day
728 0, Day 4, and Day 6 of adulthood (b), or started at Day 2 of adulthood in the DA9 (d) and NSM (e) neurons.
729 Each data point shows the average presynaptic SNG-1::ARGO GFP/RFP ratio from all the presynpases

730 in a single neuron. Curves show one-phase exponential decay functions fit to the data. Dashed black line
731 shows the experimentally calculated plateau, which comes from autofluorescence. Outlier data points that
732 were excluded from the curve calculation are shown in black. (c) SNG-1::ARGO presynaptic half-life in the
733 DA9 neuron by age, calculated from the curves shown in (b) and (d), with 95% C.I. (confidence interval).
734 (g) SNG-1 presynaptic half-life in each neuron, either averaged across all synapses or in the 10% most
735 proximal or 10% most distal synapses from the cell body, calculated from the data used to generate (d-e),
736 with 95% C.I. The DA9 data used in (f) is the same as that for Day 2 in (c).
737
738
739
740

741 ## Supplemental Material

742 **Figure S1. Validation of the "pulse" using heat-shock-promoter to express Cre recombinase.**
743 **(**a) qPCR analysis of Cre-mediated genomic recombination of the *sng-1::argo* to remove the *GFP.* The
744 animals at Time = 0 were not heat shocked. The remaining animals were heat-shocked at 34 C for one
745 hour starting at Time = 0, then returned to room temperature. Values represent fold change relative to
746 control (no heat-shock) ± SEM (n = 2 biological replicates). (b) qRT-PCR analysis of *sng-1* mRNA levels
747 with versus without the heat-shock conditions used as the "pulse" for SNG-1::ARGO shows that the pulse
748 has no significant effect on *sng-1* transcription. Values represent fold change relative to control (no heat-
749 shock) ± SEM (n = 2 biological replicates, *P<0.05, two-way ANOVA with Tukey post-test). (c-d) The heat-
750 shock "pulse" has no significant effect on SNG-1::ARGO steady-state abundance. (c) Mean presynaptic
751 SNG-1::ARGO RFP fluorescence intensity with versus without the heat-shock pulse. The experiment was
752 started on Day 2 of adulthood. Each data point shows the average mean RFP intensity for all presynapses
753 of the DA9 neuron for one neuron. (d) Number of DA9 presynapses per neuron with versus without the
754 heat shock pulse at Day 2. For (c-d), The heat-shocked animals at time = 0 were imaged 4 hours post
755 heat-shock, and bars show mean ± SEM (ns (not significant): P>0.05, *P<0.5, ***P<0.001, one-way
756 ANOVA with Tukey post-test).
757

758 **Figure S2. DNA sequence of *sng-1::argo(syb3140car2)***
759 **Figure S3. cDNA sequence of *sng-1::argo(syb3140car2)* encoding SNG-1::RFP::GFP**
760 **Figure S4. cDNA sequence of *sng-1::argo(syb3140car2)* encoding SNG-1::RFP**

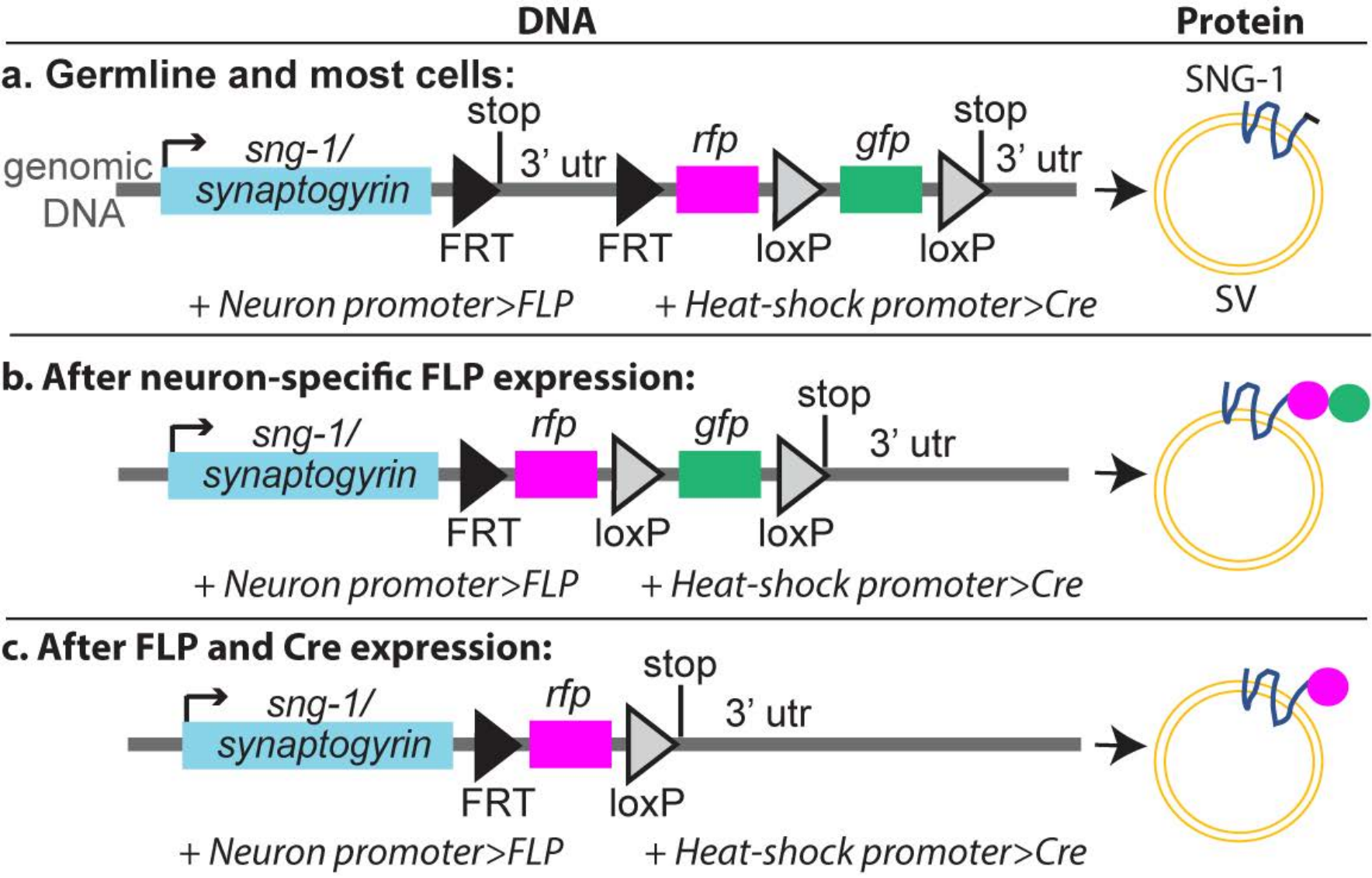
DNA
Protein
a. Germline and most cells:
genomic DNA
sng-1/ synaptogyrin
stop
3' utr
rfp
gfp
stop
3' utr
FRT
FRT
loxP
loxP
+ Neuron promoter>FLP
+ Heat-shock promoter>Cre
SNG-1
SV
b. After neuron-specific FLP expression:
sng-1/ synaptogyrin
rfp
gfp
stop
3' utr
FRT
loxP
loxP
+ Neuron promoter>FLP
+ Heat-shock promoter>Cre
c. After FLP and Cre expression:
sng-1/ synaptogyrin
rfp
stop
3' utr
FRT
loxP
+ Neuron promoter>FLP
+ Heat-shock promoter>Cre

Figure 1

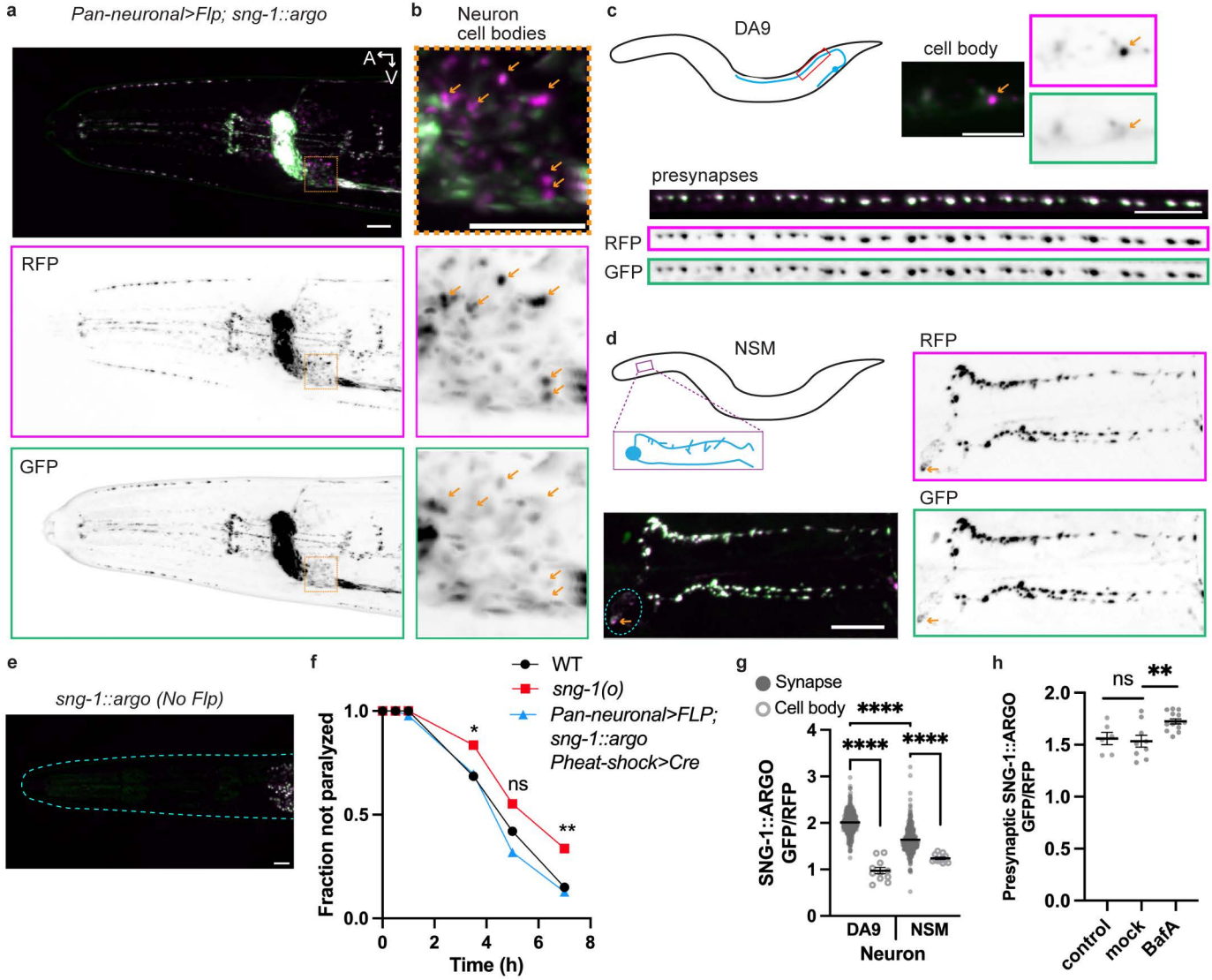
a
Pan-neuronal>Flp; sng-1::argo
A
V
RFP
GFP
b
Neuron cell bodies
c
DA9
cell body
presynapses
RFP
GFP
d
NSM
RFP
GFP
e
sng-1::argo (No Flp)
f
WT
sng-1(o)
Pan-neuronal>FLP; sng-1::argo Pheat-shock>Cre
Fraction not paralyzed
Time (h)
ns
**
g
Synapse
Cell body
****
****
****
SNG-1::ARGO GFP/RFP
DA9
NSM
Neuron
h
ns
**
Presynaptic SNG-1::ARGO GFP/RFP
control
mock
BafA

Figure 2

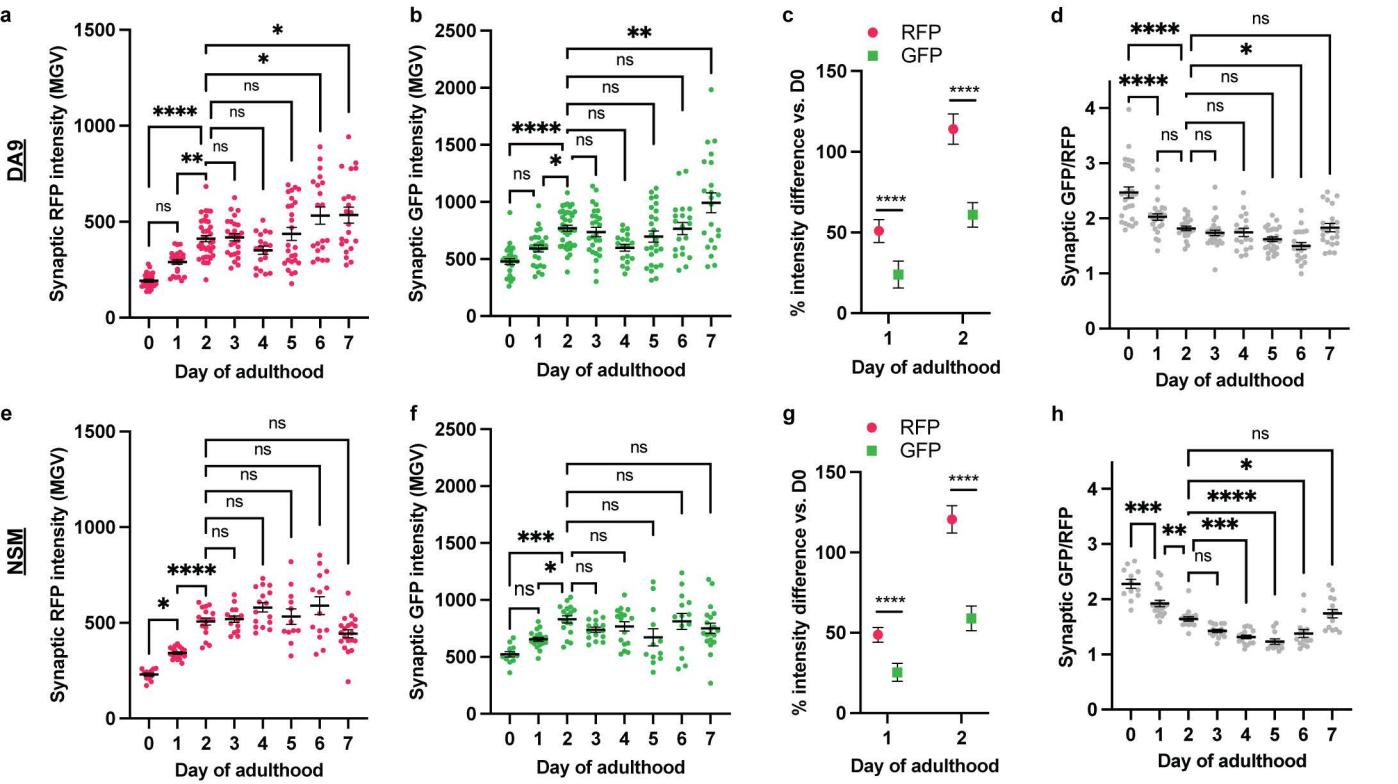
a
b
c
d
e
f
g
h
DA9
NSM
Synaptic RFP intensity (MGV)
Synaptic GFP intensity (MGV)
% intensity difference vs. D0
Synaptic GFP/RFP
Day of adulthood
RFP
GFP
ns
*
**
***
****

Figure 3

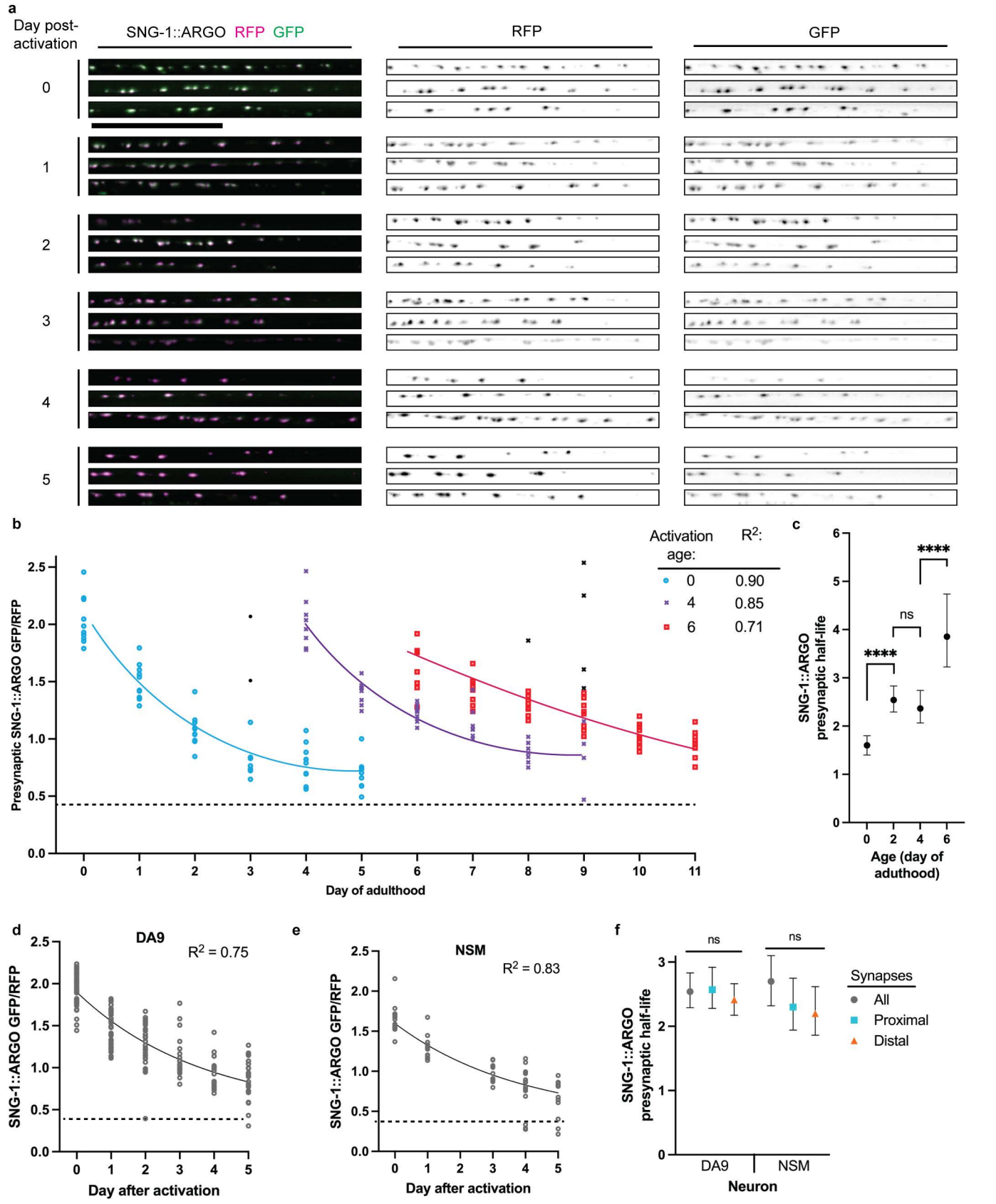
a
Day post-activation
SNG-1::ARGO RFP GFP
RFP
GFP
0
1
2
3
4
5
b
Activation age:
R2:
0 0.90
4 0.85
6 0.71
Presynaptic SNG-1::ARGO GFP/RFP
Day of adulthood
c
SNG-1::ARGO presynaptic half-life
Age (day of adulthood)
****
ns
****
d
DA9
R2 = 0.75
SNG-1::ARGO GFP/RFP
Day after activation
e
NSM
R2 = 0.83
SNG-1::ARGO GFP/RFP
Day after activation
f
ns
ns
SNG-1::ARGO presynaptic half-life
DA9
NSM
Neuron
Synapses
All
Proximal
Distal

Figure 4

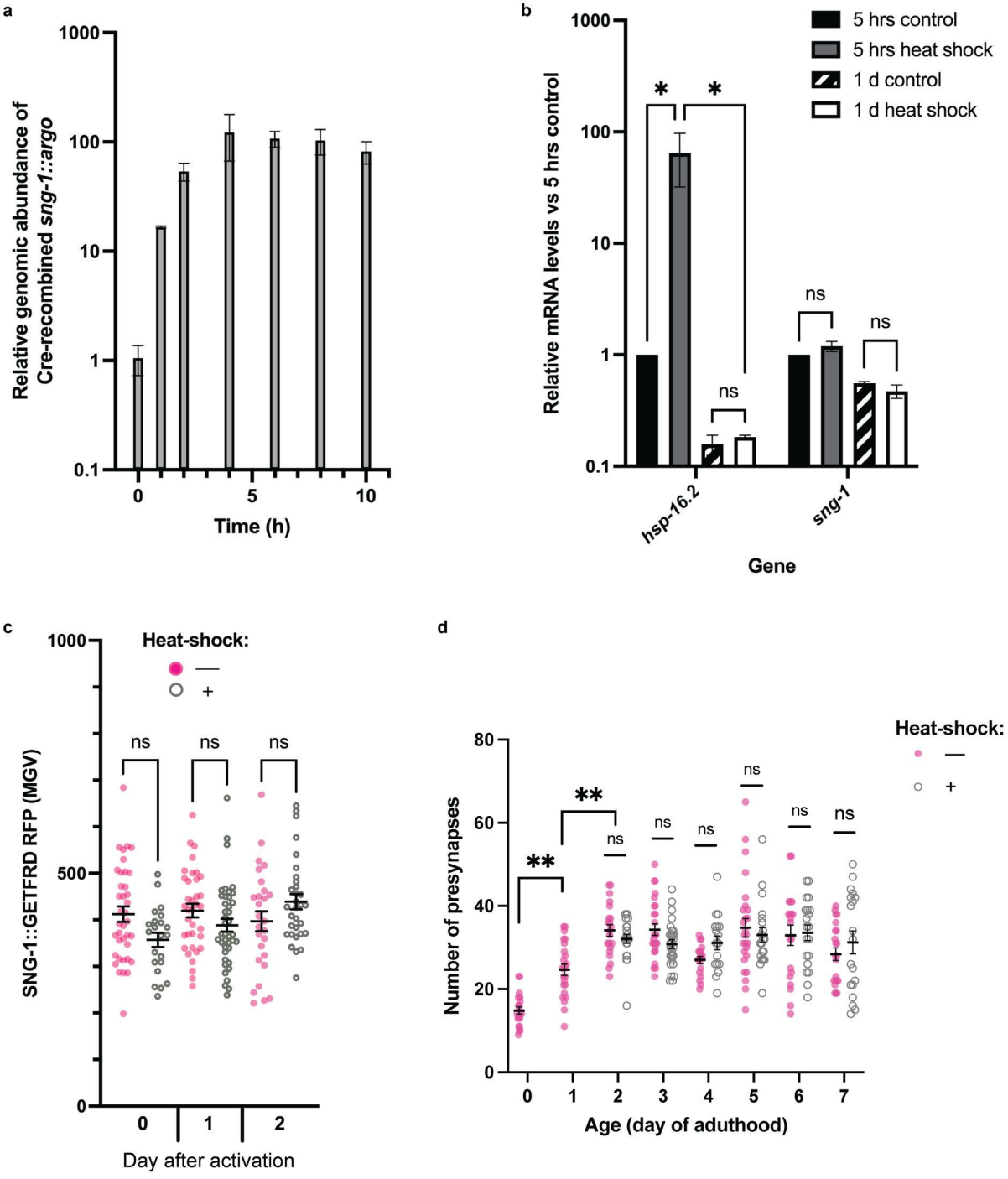
a
Relative genomic abundance of Cre-recombined sng-1::argo
1000
100
10
1
0.1
0
5
10
Time (h)
b
Relative mRNA levels vs 5 hrs control
5 hrs control
5 hrs heat shock
1 d control
1 d heat shock
*
*
ns
ns
ns
hsp-16.2
sng-1
Gene
c
Heat-shock:
—
+
SNG-1::GETFRD RFP (MGV)
ns
ns
ns
Day after activation
d
Heat-shock:
—
+
Number of presynapses
**
**
ns
Age (day of aduthood)

Figure S1

(from 1-749 bp)

sng-1 syb3140car2 genomic locus (2457 bp)

```
GCAACAACCACCATCAAACCCATAtACTCAaTCgGAAGGATATGGTTATGGAAGTTCCTATTCTCTAGAAAGTATAGGAACTTCATAAattttcaaattttaaatac
CGTTGTTGGTGGTAGTTTGGGTATaTGAGTtAGcCTTCCTATACCAATACCTTCAAGGATAAGAGATCTTTCATATCCTTGAAGTATTtaaaagtttaaaatttatg
```

FRT | 3' utr

10 20 30 40 50 60 70 80 90 100

```
tgaatatttgtttttttcctattatttatttattctctttgtgtttttttcttgctttctaaaaaattaattcaatccaaatctaaacatttttttttctctttc
acttataaacaaaaaaaggataataaataaataagagaaacacaaaaaaaagaacgaaagatttttttaattaagttaggtttagatttgtaaaaaaaaagagaaag
```

3' utr

110 120 130 140 150 160 170 180 190 200 210

```
cgtctcccaattcgtattccgctcctctcatctgaacacaatgtgcaagtttatttatcttctcgctttcatttcattaggacgtgggggggaattggtggaaggggg
gcagagggttaagcataaggcgaggagagtagacttgtgttacacgttcaaataaatagaagagcgaaagtaaagtaatcctgcaccccccttaaccaccttccccc
```

3' utr

220 230 240 250 260 270 280 290 300 310 320

```
aaacacacaaaaggatgatggaaatgaaataaggacacacaatatgcaacaacattcaattcagaaatatggaggaaggtttaaaagaaaacataaaaatatataga
tttgtgtgttttcctactacctttactttattcctgtgtgttatacgttgttgtaagttaagtctttatacctccttccaaattttcttttgtatttttatatatct
```

3' utr

330 340 350 360 370 380 390 400 410 420

```
ggaggaaggaaaactagtaaaaaataagcaaagaaattaggcgaacgatgagaattgtcctcgcttgGAAGTTCCTATTCTCTAGAAAGTATAGGAACTTCAGTCTC
cctccttccttttgatcatttttttattcgtttctttaatccgcttgctactcttaacaggagcgaacCTTCAAGGATAAGAGATCTTTCATATCCTTGAAGTCAGAG
```

1 2
V S

3' utr | FRT

430 440 450 460 470 480 490 500 510 520 530

```
CAAGGGAGAGGAGCTCATCAAGGAGAACATGCACATGAAGCTCTACATGGAGGGAACCGTCAACAACCACCACTTCAAGTGCACCTCCGAGGGAGAGGGAAAGCCAT
GTTCCCTCTCCTCGAGTAGTTCCTCTTGTACGTGTACTTCGAGATGTACCTCCCTTGGCAGTTGTTGGTGGTGAAGTTCACGTGGAGGCTCCCTCTCCCTTTCGGTA
```

3 4 5 6 7 8 9 10 11 12 13 14 15 16 17 18 19 20 21 22 23 24 25 26 27 28 29 30 31 32 33 34 35 36 37
K G E E L I K E N M H M K L Y M E G T V N N H H F K C T S E G E G K P
tagRFP

540 550 560 570 580 590 600 610 620 630 640

```
ACGAGGGAACCCAAACCATGCGTATCAAGGtaagtttaaacatatatatactaactaaccctgattatttaaattttcaggTCGTCGAGGGAGGACCACTCCCATTC
TGCTCCCTTGGGTTTGGTACGCATAGTTCCattcaaatttgtatatatatgattgattgggactaataaatttaaaagtccAGCAGCTCCCTCCTGGTGAGGGTAAG
```

38 39 40 41 42 43 44 45 46 47
Y E G T Q T M R I K
tagRFP

1 2 3 4 5 6 7 8 9
S S R E D H S H S
tagRFP

intron

650 660 670 680 690 700 710 720 730 740

sng-1 syb3140car2 genomic locus (2457 bp) (from 750-1391 bp)

```
GCCTTCGACATCCTCGCCACCTCCTTCATGTACGGATCCCGTACCTTCATCAACCACACCCAAGGAATCCCAGACTTCTTCAAGCAATCCTTCCCAGAGGGATTCAC
CGGAAGCTGTAGGAGCGGTGGAGGAAGTACATGCCTAGGGCATGGAAGTAGTTGGTGTGGGTTCCTTAGGGTCTGAAGAAGTTCGTTAGGAAGGGTCTCCCTAAGTG
 10 11 12 13 14 15 16 17 18 19 20 21 22 23 24 25 26 27 28 29 30 31 32 33 34 35 36 37 38 39 40 41 42 43 44
  P  S  T  S  S  P  P  P  S  C  T  D  P  V  P  S  S  T  T  P  K  E  S  Q  T  S  S  S  N  P  S  Q  R  D  S
tagRFP

750       760       770       780       790       800       810       820       830       840       850

CTGGGAGCGTGTCACCACCTACGAGGACGGAGGAGTCCTCACCGCCACCCAAGACACCTCCCTCCAAGACGGATGCCTCATCTACAACGTCAAGgtaagtttaaaca
GACCCTCGCACAGTGGTGGATGCTCCTGCCTCCTCAGGAGTGGCGGTGGGTTCTGTGGAGGGAGGTTCTGCCTACGGAGTAGATGTTGCAGTTCcattcaaatttgt
45 46 47 48 49 50 51 52 53 54 55 56 57 58 59 60 61 62 63 64 65 66 67 68 69 70 71 72 73 74 75
 P  G  S  V  S  P  P  T  R  T  E  E  S  S  P  P  P  K  T  P  P  S  K  T  D  A  S  S  T  T  S
tagRFP

                                                                                                  intron

860       870       880       890       900       910       920       930       940       950       960

gttcggtactaactaaccatacatatttaaattttcagATCCGTGGAGTCAACTTCCCATCCAACGGACCAGTCATGCAAAAGAAGACCCTCGGATGGGAGGCCAAC
caagccatgattgattggtatgtataaatttaaaagtcTAGGCACCTCAGTTGAAGGGTAGGTTGCCTGGTCAGTACGTTTTCTTCTGGGAGCCTACCCTCCGGTTG
                                       1  2  3  4  5  6  7  8  9 10 11 12 13 14 15 16 17 18 19 20 21 22 23
                                       I  R  G  V  N  F  P  S  N  G  P  V  M  Q  K  K  T  L  G  W  E  A  N
                                       tagRFP

                  intron

970       980       990      1,000     1,010     1,020     1,030     1,040     1,050     1,060     1,070

ACCGAGATGCTCTACCCAGCCGACGGAGGACTcGAGGGACGTACCGACATGGCCCTCAAGCTCGTCGGAGGAGGACACCTCATCTGCAACTTCAAGACCACCTACCG
TGGCTCTACGAGATGGGTCGGCTGCCTCCTGAgCTCCCTGCATGGCTGTACCGGGAGTTCGAGCAGCCTCCTCCTGTGGAGTAGACGTTGAAGTTCTGGTGGATGGC
24 25 26 27 28 29 30 31 32 33 34 35 36 37 38 39 40 41 42 43 44 45 46 47 48 49 50 51 52 53 54 55 56 57 58 59
 T  E  M  L  Y  P  A  D  G  G  L  E  G  R  T  D  M  A  L  K  L  V  G  G  G  H  L  I  C  N  F  K  T  T  Y  R
tagRFP

      1,080     1,090     1,100     1,110     1,120     1,130     1,140     1,150     1,160     1,170

TTCCAAGgtaagtttaaacatgattttactaactaactaatctgatttaaattttcagAAGCCAGCCAAGAACCTCAAGATGCCAGGAGTCTACTACGTCGACCACC
AAGGTTCcattcaaatttgtactaaaatgattgattgattagactaaatttaaaagtcTTCGGTCGGTTCTTGGAGTTCTACGGTCCTCAGATGATGCAGCTGGTGG
 60                                                        1  2  3  4  5  6  7  8  9 10 11 12 13 14 15 16
  S                                                        K  P  A  K  N  L  K  M  P  G  V  Y  Y  V  D  H
                                                           tagRFP

                                  intron

1,180     1,190     1,200     1,210     1,220     1,230     1,240     1,250     1,260     1,270     1,280

GTCTcGAGCGTATCAAGGAGGCCGACAAGGAGACcTACGTCGAGCAACACGAGGTCGCCGTCGCCCGTTACTGCGACCTCCCATCCAAGCTCGGACACAAGCTCAAC
CAGAgCTCGCATAGTTCCTCCGGCTGTTCCTCTGgATGCAGCTCGTTGTGCTCCAGCGGCAGCGGGCAATGACGCTGGAGGGTAGGTTCGAGCCTGTGTTCGAGTTG
17 18 19 20 21 22 23 24 25 26 27 28 29 30 31 32 33 34 35 36 37 38 39 40 41 42 43 44 45 46 47 48 49 50 51 52
 R  L  E  R  I  K  E  A  D  K  E  T  Y  V  E  Q  H  E  V  A  V  A  R  Y  C  D  L  P  S  K  L  G  H  K  L  N
tagRFP

      1,290     1,300     1,310     1,320     1,330     1,340     1,350     1,360     1,370     1,380     1,390
```

sng-1 syb3140car2 genomic locus (2457 bp) (from 1392-2033 bp)

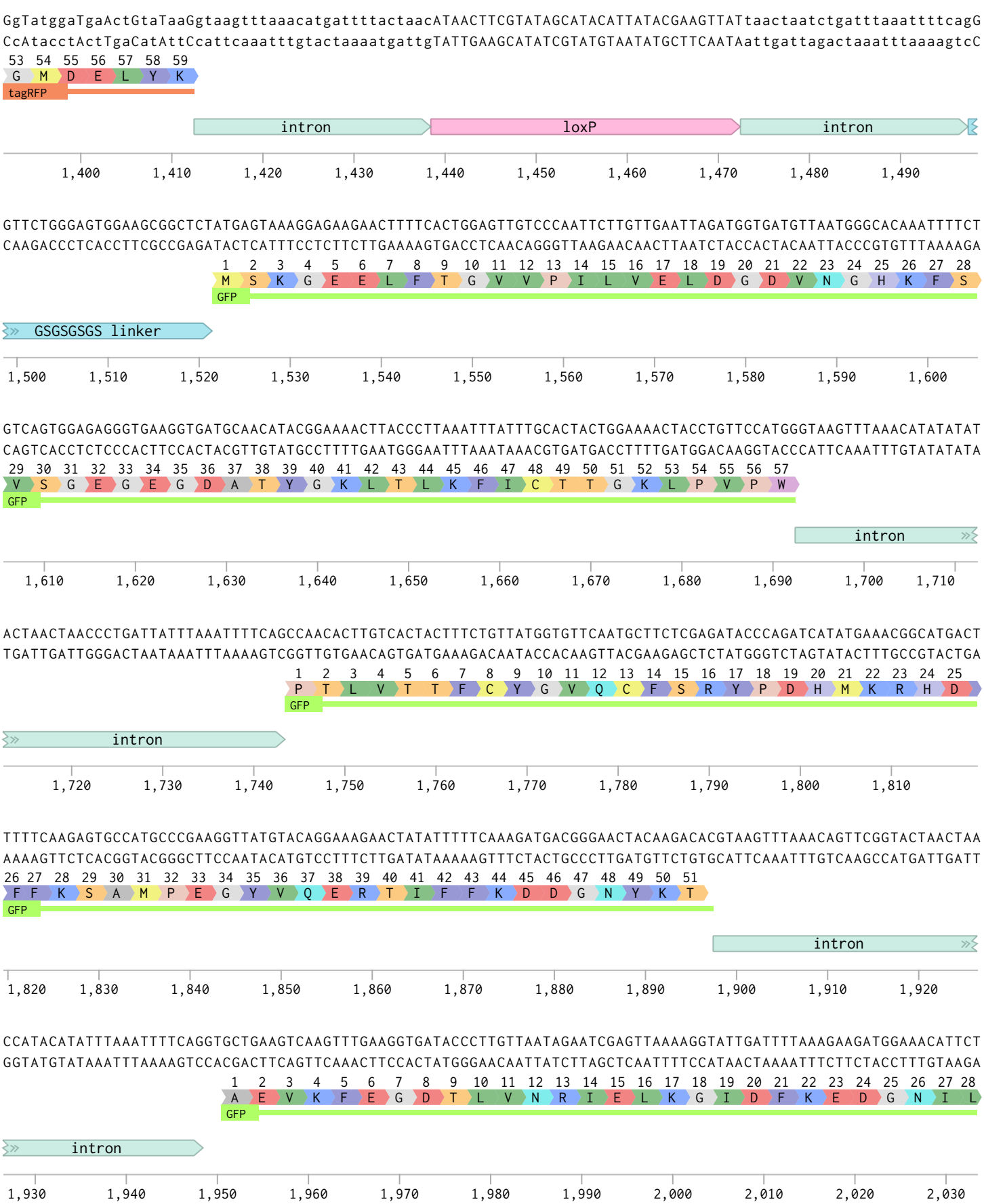

sng-1 syb3140car2 genomic locus (2457 bp) (from 2034-2457 bp)

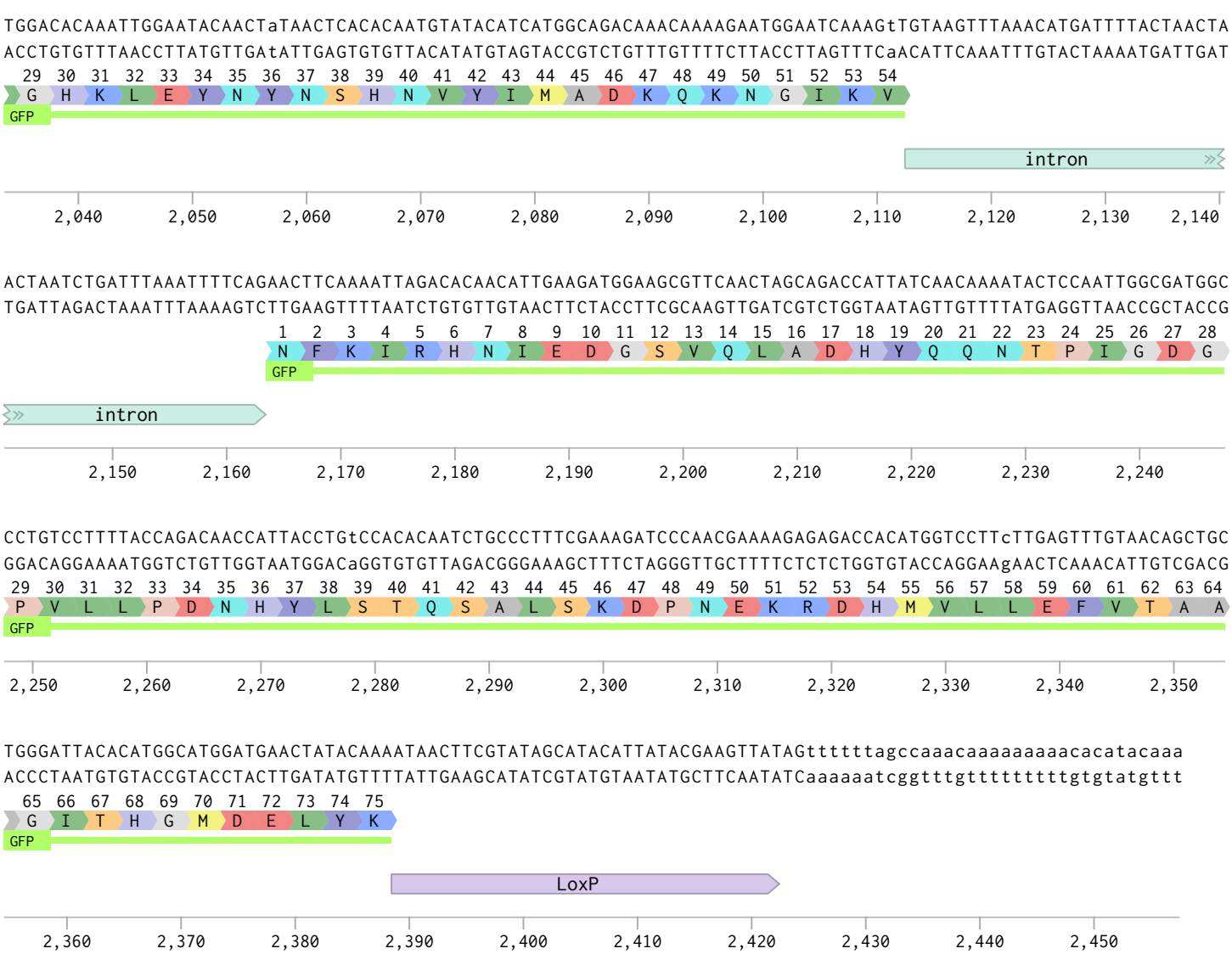

Fig S2

(from 1-415 bp)

cDNA sng-1 syb3140car2 (1619 bp)

```
CCATGCAACAACCACCATCAAACCCATAtACTCAaTCgGAAGGATATGGTTATGGAAGTTCCTATTCTCTAGAAAGTATAGGA
GGTACGTTGTTGGTGGTAGTTTGGGTATaTGAGTtAGcCTTCCTATACCAATACCTTCAAGGATAAGAGATCTTTCATATCCT
```

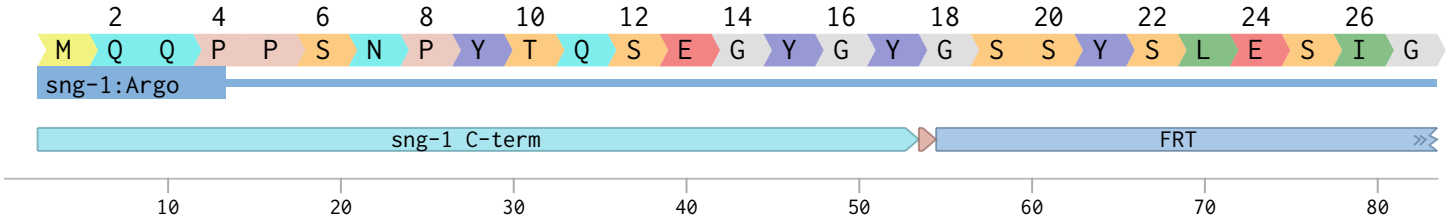


```
ACTTCAGTCTCCAAGGGAGAGGAGCTCATCAAGGAGAACATGCACATGAAGCTCTACATGGAGGGAACCGTCAACAACCACCA
TGAAGTCAGAGGTTCCCTCTCCTCGAGTAGTTCCTCTTGTACGTGTACTTCGAGATGTACCTCCCTTGGCAGTTGTTGGTGGT
```

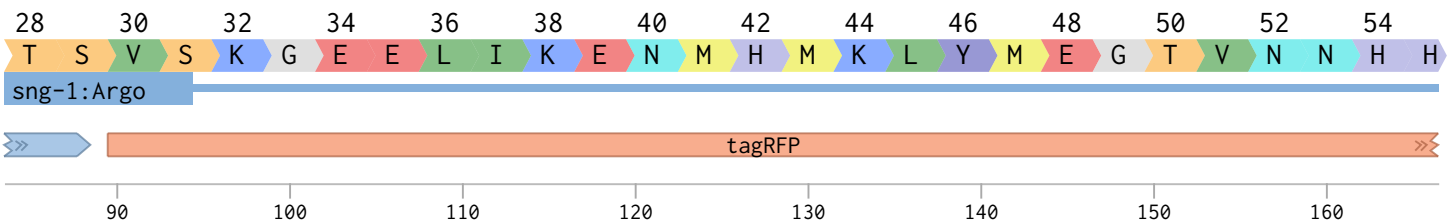


```
CTTCAAGTGCACCTCCGAGGGAGAGGGAAAGCCATACGAGGGAACCCAAACCATGCGTATCAAGTCGTCGAGGGAGGACCACT
GAAGTTCACGTGGAGGCTCCCTCTCCCTTTCGGTATGCTCCCTTGGGTTTGGTACGCATAGTTCAGCAGCTCCCTCCTGGTGA
```

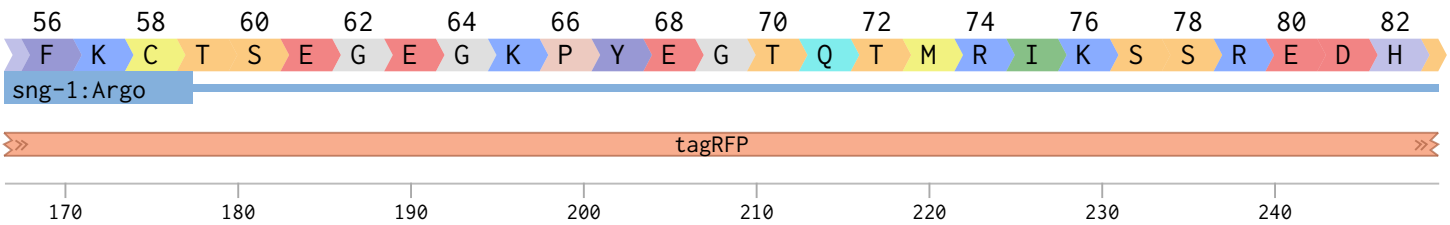


```
CCCATTCGCCTTCGACATCCTCGCCACCTCCTTCATGTACGGATCCCGTACCTTCATCAACCACACCCAAGGAATCCCAGACT
GGGTAAGCGGAAGCTGTAGGAGCGGTGGAGGAAGTACATGCCTAGGGCATGGAAGTAGTTGGTGTGGGTTCCTTAGGGTCTGA
```

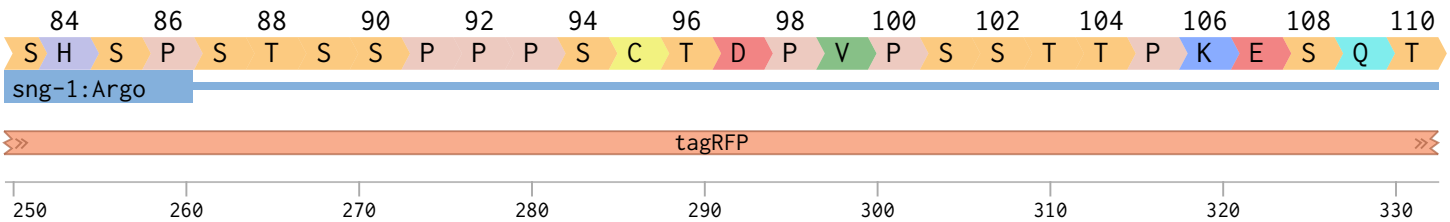


```
TCTTCAAGCAATCCTTCCCAGAGGGATTCACCTGGGAGCGTGTCACCACCTACGAGGACGGAGGAGTCCTCACCGCCACCCAA
AGAAGTTCGTTAGGAAGGGTCTCCCTAAGTGGACCCTCGCACAGTGGTGGATGCTCCTGCCTCCTCAGGAGTGGCGGTGGGTT
```

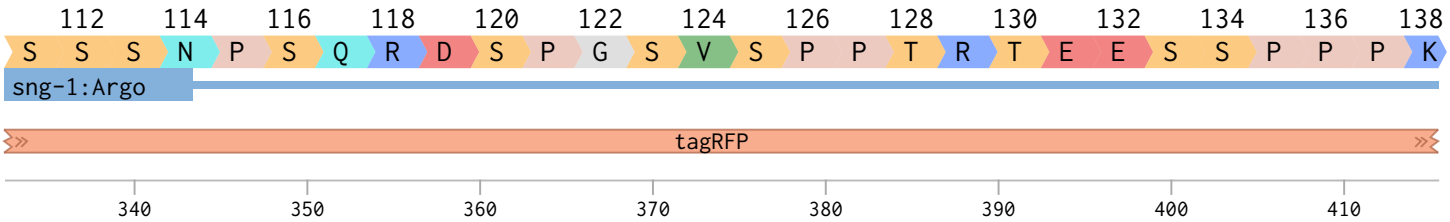

cDNA sng-1 syb3140car2 (1619 bp) (from 416-830 bp)

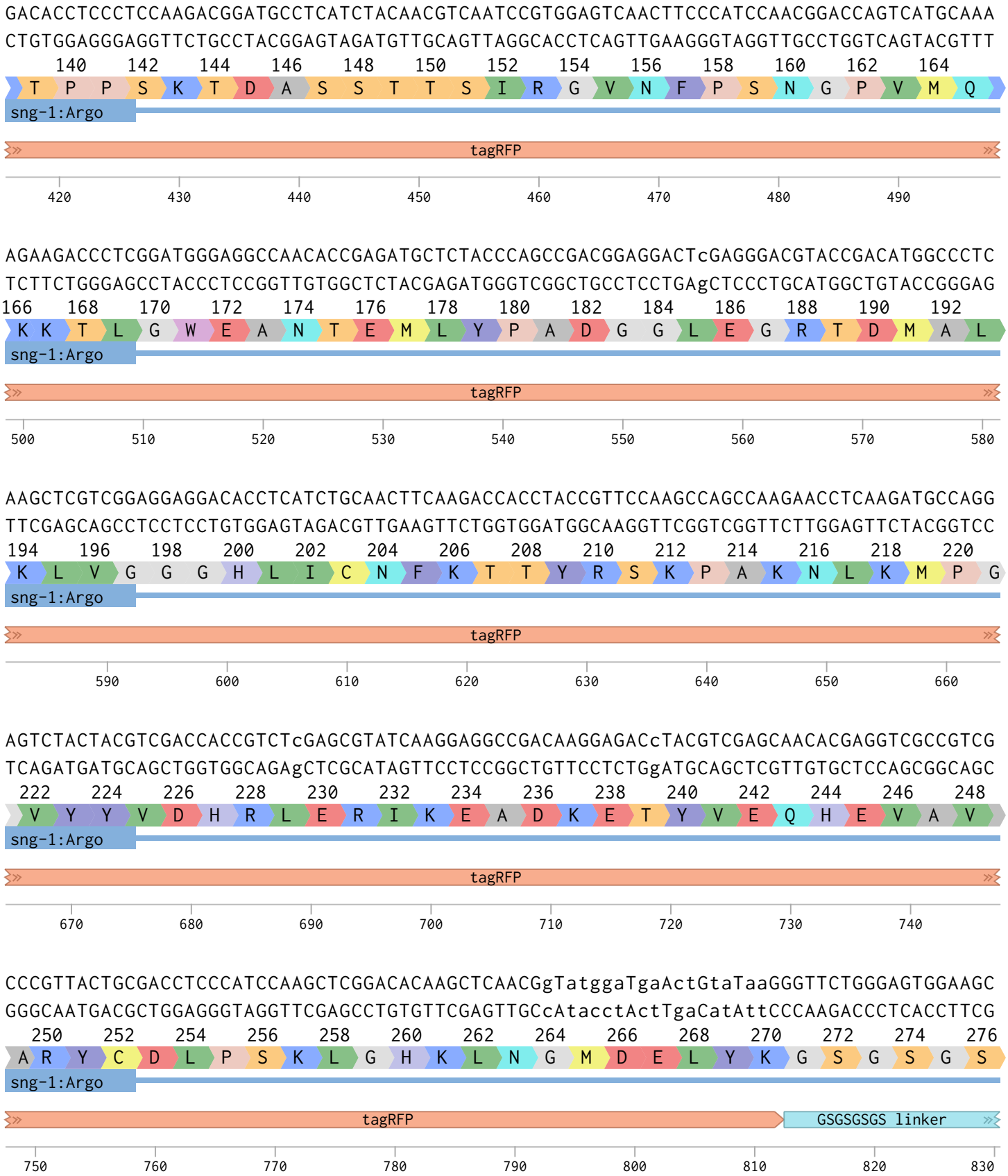

cDNA sng-1 syb3140car2 (1619 bp) (from 831-1245 bp)

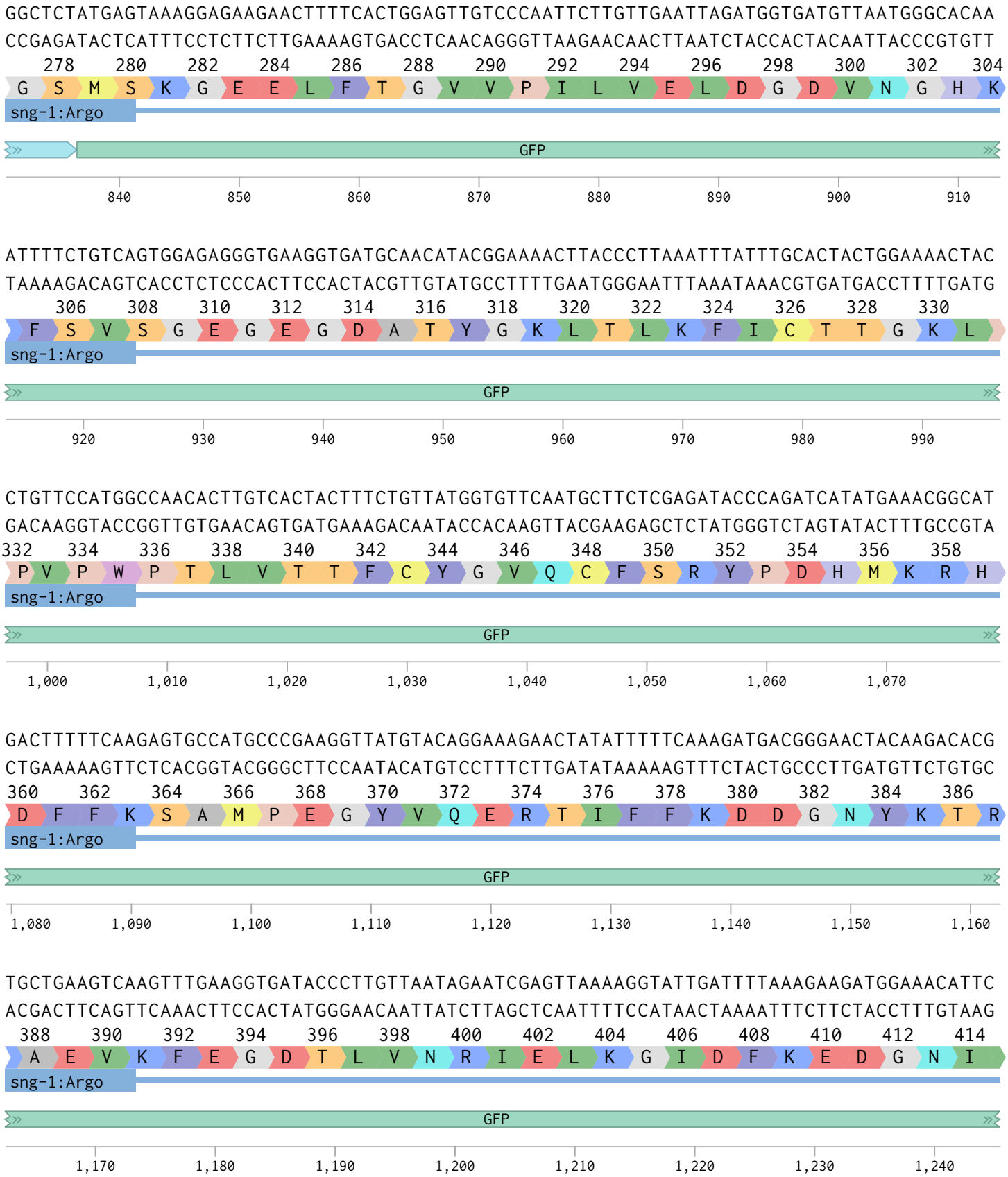

cDNA sng-1 syb3140car2 (1619 bp) (from 1246-1619 bp)

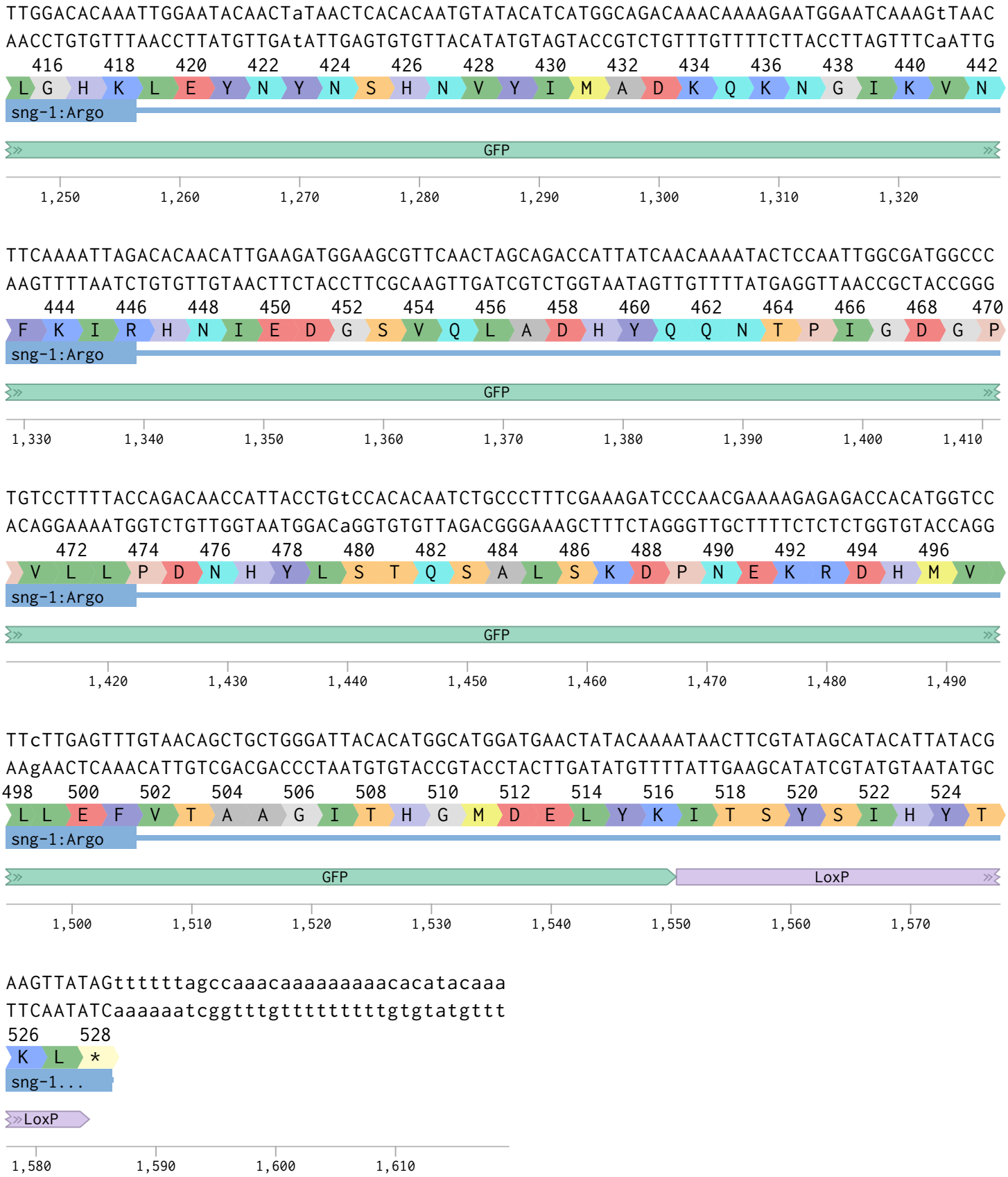

Figure S3

(from 1-465 bp)

syb3140car2 recombined (891 bp)

```
CCATGCAACAACCACCATCAAACCCATAtACTCAaTCgGAAGGATATGGTTATGGAAGTTCCTATTCTCTAGAAAGTATAGGAACTTCAGTCT
GGTACGTTGTTGGTGGTAGTTTGGGTATaTGAGTtAGcCTTCCTATACCAATACCTTCAAGGATAAGAGATCTTTCATATCCTTGAAGTCAGA
      2    4    6    8   10   12   14   16   18   20   22   24   26   28   30
      M    Q    Q    P    P    S    N    P    Y    T    Q    S    E    G    Y    G    Y    G    S    S    Y    S    L    E    S    I    G    T    S    V
      Translation

      sng-1 C-term                                                                  FRT
                                                                                    »

                10        20        30        40        50        60        70        80        90
```

```
CCAAGGGAGAGGAGCTCATCAAGGAGAACATGCACATGAAGCTCTACATGGAGGGAACCGTCAACAACCACCACTTCAAGTGCACCTCCGAGG
GGTTCCCTCTCCTCGAGTAGTTCCTCTTGTACGTGTACTTCGAGATGTACCTCCCTTGGCAGTTGTTGGTGGTGAAGTTCACGTGGAGGCTCC
  32   34   36   38   40   42   44   46   48   50   52   54   56   58   60
  S    K    G    E    E    L    I    K    E    N    M    H    M    K    L    Y    M    E    G    T    V    N    N    H    H    F    K    C    T    S    E
  Translation

  »                                                                                                                                                  »
                                                                  tagRFP

                100       110       120       130       140       150       160       170       180
```

```
GAGAGGGAAAGCCATACGAGGGAACCCAAACCATGCGTATCAAGGTCGTCGAGGGAGGACCACTCCCATTCGCCTTCGACATCCTCGCCACCT
CTCTCCCTTTCGGTATGCTCCCTTGGGTTTGGTACGCATAGTTCCAGCAGCTCCCTCCTGGTGAGGGTAAGCGGAAGCTGTAGGAGCGGTGGA
62   64   66   68   70   72   74   76   78   80   82   84   86   88   90   92
G    E    G    K    P    Y    E    G    T    Q    T    M    R    I    K    V    V    E    G    G    P    L    P    F    A    F    D    I    L    A    T
Translation

»                                                                                                                                                  »
                                                                  tagRFP

                190       200       210       220       230       240       250       260       270
```

```
CCTTCATGTACGGATCCCGTACCTTCATCAACCACACCCAAGGAATCCCAGACTTCTTCAAGCAATCCTTCCCAGAGGGATTCACCTGGGAGC
GGAAGTACATGCCTAGGGCATGGAAGTAGTTGGTGTGGGTTCCTTAGGGTCTGAAGAAGTTCGTTAGGAAGGGTCTCCCTAAGTGGACCCTCG
  94   96   98  100  102  104  106  108  110  112  114  116  118  120  122
  S    F    M    Y    G    S    R    T    F    I    N    H    T    Q    G    I    P    D    F    F    K    Q    S    F    P    E    G    F    T    W    E
  Translation

  »                                                                                                                                                  »
                                                                  tagRFP

                280       290       300       310       320       330       340       350       360       370
```

```
GTGTCACCACCTACGAGGACGGAGGAGTCCTCACCGCCACCCAAGACACCTCCCTCCAAGACGGATGCCTCATCTACAACGTCAAGATCCGTG
CACAGTGGTGGATGCTCCTGCCTCCTCAGGAGTGGCGGTGGGTTCTGTGGAGGGAGGTTCTGCCTACGGAGTAGATGTTGCAGTTCTAGGCAC
124  126  128  130  132  134  136  138  140  142  144  146  148  150  152  154
R    V    T    T    Y    E    D    G    G    V    L    T    A    T    Q    D    T    S    L    Q    D    G    C    L    I    Y    N    V    K    I    R
Translation

»                                                                                                                                                  »
                                                                  tagRFP

                380       390       400       410       420       430       440       450       460
```

syb3140car2 recombined (891 bp) (from 466-891 bp)

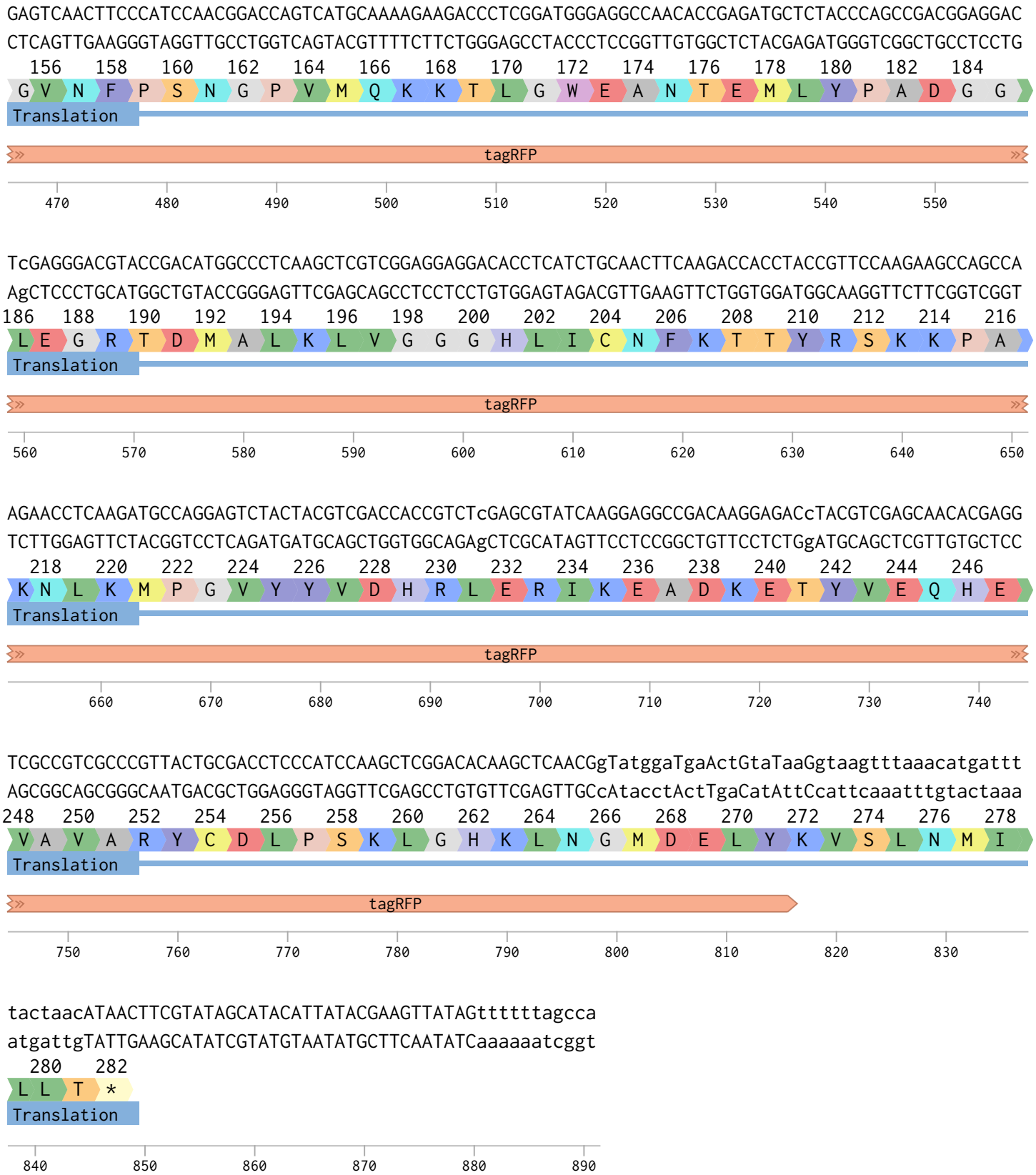

Fig S4